




## ARTICLE

# Developing T cells form an immunological synapse for passage through the $\beta$ -selection checkpoint

Amr H. Allam<sup>1,2</sup> , Mirren Charnley<sup>1,2</sup> , Kim Pham<sup>1,2,3</sup>, and Sarah M. Russell<sup>1,2,3,4</sup> 

The  $\beta$ -selection checkpoint of T cell development tests whether the cell has recombined its genomic DNA to produce a functional T cell receptor  $\beta$  (TCR $\beta$ ). Passage through the  $\beta$ -selection checkpoint requires the nascent TCR $\beta$  protein to mediate signaling through a pre-TCR complex. In this study, we show that developing T cells at the  $\beta$ -selection checkpoint establish an immunological synapse *in vitro* and *in situ*, resembling that of the mature T cell. The immunological synapse is dependent on two key signaling pathways known to be critical for the transition beyond the  $\beta$ -selection checkpoint, Notch and CXCR4 signaling. *In vitro* and *in situ* analyses indicate that the immunological synapse promotes passage through the  $\beta$ -selection checkpoint. Collectively, these data indicate that developing T cells regulate pre-TCR signaling through the formation of an immunological synapse. This signaling platform integrates cues from Notch, CXCR4, and MHC on the thymic stromal cell to allow transition beyond the  $\beta$ -selection checkpoint.

## Introduction

Mature T cells each express a unique T cell receptor (TCR) to enable binding and response to specific antigens (Smith-Garvin et al., 2009; Turner et al., 2006). The TCR is created by genomic recombination during T cell development in the thymus (Mallick et al., 1993; Pardoll et al., 1987). To ensure that its TCR is fit for purpose, the developing T cell must survive a series of tests. The first of these tests, termed the  $\beta$ -selection checkpoint, assesses whether the developing T cell has recombined its TCR $\beta$  gene appropriately (Carpenter and Bosselut, 2010). Much has been learned about the signaling and cell fate decisions that depend upon correct TCR $\beta$  recombination at this stage (Chan and Russell, 2019). At the  $\beta$ -selection checkpoint, the T cell still lacks a recombined TCR $\alpha$  but pairs with the pre-TCR $\alpha$  (pT $\alpha$ ) chain (Groettrup et al., 1993; Raulet et al., 1985). The nascent TCR $\beta$  paired with pT $\alpha$  is termed a pre-TCR and shares many characteristics with the TCR of mature T cells, including association with CD3 and associated cell surface receptors and triggering of similar signaling cascades (Saint-Ruf et al., 2000; von Boehmer, 2005).

The vast literature on mechanisms of action of the TCR in mature cells has provided a platform for understanding the mechanisms of pre-TCR signaling, but not all characteristics are shared between the two TCR types (Gascoigne et al., 2016). The

most profound differences relate to the impact of ligand binding on higher-order organization of signaling. In a mature T cell, interaction of the TCR with antigen presented via major histocompatibility complex (MHC) triggers a highly orchestrated spatial reorganization (Alcover et al., 2016; Martín-Cófreces et al., 2011). This reorganization involves assembly of a dynamic structure termed the immunological synapse, which enables control over the intensity and duration of the antigen presentation signal during T cell activation and T cell-mediated killing of target cells (Dustin et al., 2010; Lee et al., 2002, 2003). A similar structure has not been considered in developing T cells, in part because the lack of a genomically rearranged TCR $\alpha$  chain at the  $\beta$ -selection checkpoint means that the cell cannot undergo canonical binding to peptide-MHC complexes (Mallick et al., 1993). In place of ligand binding and formation of an immunological synapse, models for activation of the pre-TCR initially relied upon the notion that dimerization of TCR $\beta$  with pT $\alpha$  stabilizes the protein, paving the way for lipid-raft-based clustering to initiate signaling (Saint-Ruf et al., 2000). However, a number of studies showed that the cysteine residue in the pT $\alpha$  cytoplasmic domain, which is involved in the palmitoylation site, is not required for the transition from double negative (DN; cells lack CD4 and CD8 surface expression) to double positive (DP;

<sup>1</sup>Optical Sciences Centre, Faculty of Science, Engineering & Technology, Swinburne University of Technology, Hawthorn, Victoria, Australia; <sup>2</sup>Immune Signalling Laboratory, Peter MacCallum Cancer Centre, Parkville, Victoria, Australia; <sup>3</sup>Department of Pathology, The University of Melbourne, Australia; <sup>4</sup>Sir Peter MacCallum Department of Oncology, The University of Melbourne, Australia.

Correspondence to Sarah Russell: [sarah.russell@petermac.org](mailto:sarah.russell@petermac.org); A.H. Allam's present address is Cancer and Inflammation Laboratory, Olivia Newton-John Cancer Research Institute and School of Cancer Medicine, La Trobe University, Heidelberg, Victoria, Australia; K. Pham's present address is Division of Immunology, The Walter and Eliza Hall Institute of Medical Research, Parkville, Victoria, Australia, and Department of Medical Biology, The University of Melbourne, Parkville, Victoria, Australia.

© 2021 Allam et al. This article is distributed under the terms of an Attribution–Noncommercial–Share Alike–No Mirror Sites license for the first six months after the publication date (see <http://www.rupress.org/terms/>). After six months it is available under a Creative Commons License (Attribution–Noncommercial–Share Alike 4.0 International license, as described at <https://creativecommons.org/licenses/by-nc-sa/4.0/>).

cells acquired CD4 and CD8 surface expression) stages (Aifantis et al., 2002). Moreover, CD3 $\epsilon$  dimerization was sufficient for progression beyond  $\beta$ -selection even when there was no raft localization (Levelt et al., 1995; Shinkai et al., 1995). Later studies showed that the pT $\alpha$  extracellular domain undergoes self-oligomerization via four charged amino acids that are required for initiation of the pre-TCR signaling and progression beyond the  $\beta$ -selection (Pang et al., 2010; Yamasaki et al., 2006). On the other hand, signal initiation of the pre-TCR does not require oligomerization but rather depends on regulating the surface expression of the pre-TCR complexes and their abundance (Mahtani-Patching et al., 2011). Thus, there is not yet a clear consensus as to what triggers productive signaling through the pre-TCR.

It is becoming apparent that signaling through the pre-TCR might be more akin to signaling through the TCR of mature T cells than had previously been considered. Recent findings indicate that the pre-TCR can bind peptide-MHC complexes and that signaling from the peptide-MHC complex can influence T cell development (Das et al., 2016; Mallis et al., 2015). The affinity of the interaction is lower than that of the  $\alpha\beta$  TCR (Mallis et al., 2015), suggesting the possibility that binding of the pre-TCR might require facilitation by other molecules. We and others have previously found that the interaction between stromal cells and developing T cells at the  $\beta$ -selection checkpoint involves recruitment of the microtubule organizing center (MTOC), a hallmark of initiation of the immunological synapse (Charnley et al., 2019; Martín-Cófreces et al., 2008; Pham et al., 2015). This finding, combined with the interaction between pre-TCR and stromal cell MHC, opened the possibility that an immunological synapse might facilitate TCR signaling during  $\beta$ -selection.

Here, we demonstrate that the developing T cell indeed does form an immunological synapse upon interaction with stromal cells during  $\beta$ -selection. We characterize the synapse in *in vitro* T cell cultures and *in situ* in an intact mouse thymus. We further show that establishment of the synapse relies upon cooperation between pre-TCR and two key signaling pathways, Notch and CXCR4 signaling, which are essential for robust progression beyond the  $\beta$ -selection (Ciofani et al., 2004; Janas et al., 2010; Maillard et al., 2006; Trampont et al., 2010; Wolfer et al., 2002). Finally, we demonstrate that the immunological synapse is a prerequisite for proliferation following the  $\beta$ -selection checkpoint.

## Results

### DN3 cells make an immunological synapse *in vitro* and *in situ*

Our previous observation that the MTOC was recruited to the interface with the stromal cell (Charnley et al., 2019; Pham et al., 2015), reminiscent of an immunological synapse in mature cells (Alcover et al., 2016; Dustin and Baldari, 2017), led us to assess whether developing T cells might also form an immunological synapse. Flow cytometry confirmed that pre-TCR components, including the pT $\alpha$  chain, TCR $\beta$  chain, LCK, LAT, and PKC $\theta$ , were expressed in DN3 cells. Phosphorylation of the TCR-associated kinase LCK (pLCK<sup>394</sup> and pLCK<sup>505</sup> [active and inactive forms, respectively]) and ZAP70 (pZAP70) in DN3 cells indicated active

signaling through the pre-TCR (Fig. S1). To assess the localization of pre-TCR components, we incubated *in vitro*-generated DN3 cells with OP9-DL1 stromal cells and analyzed conjugates by immunofluorescence. Blinded scoring indicated that pT $\alpha$  and TCR $\beta$  were polarized in most conjugates (61.4% and 84.6% respectively; Fig. 1, A and B). Engagement of the TCR in mature T cells initiates downstream signal transduction with polarization of its downstream signaling molecules and phosphorylation of the immunoreceptor tyrosine-based motifs (Alarcón et al., 2011; Alcover et al., 2016; Gaud et al., 2018). Similarly for the developing T cells, the majority of conjugates showed polarization of total LCK (86.5%), pLCK<sup>394</sup> (71.6%), pLCK<sup>505</sup> (86.8%), pZAP70 (52.1%), and LAT (75.6%). Interestingly, and in contrast to mature T cells, PKC $\theta$  was rarely found to be polarized (28.3%). Together, these findings indicate that developing T cells cluster TCR components at the interface with the stromal cells during the TCR $\beta$  checkpoint.

The above findings suggest that developing T cells form the equivalent of an immunological synapse. To ensure that these findings were not an artifact of the OP9-DL1 stromal system, we assessed the localization of TCR components in an intact thymus. We used six-color immunofluorescence imaging to investigate polarization of pT $\alpha$ , and pLCK<sup>394</sup> in the DN3 population (Fig. 1, C–E). As previously found (Charnley et al., 2019; Pham et al., 2015), the cytokine receptor CD25 was not polarized (Fig. 1 C). However, pT $\alpha$  was polarized in 58.6% and pLCK<sup>394</sup> in 62.6% of DN3 cells in the thymus. These data suggest that developing T cells form a structure at the interface with stromal cells that is similar to the immunological synapse of mature T cells. This structure involves clustered pre-TCR and associated signaling molecules and is observed both in DN3a cells docking onto OP9-DL1 stromal cells and *in situ* in an intact thymus.

### The DN3 immunological synapse is stable for up to 2 h and involves reorientation of MTOC coincident with recruitment of LAT

To assess the dynamics of the clustering at the interface, we used fluorescence time-lapse microscopy. We stained purified DN3a cells for F-actin using the SiR-Actin live dye, and we used confocal microscopy to image DN3a cells docking onto OP9-DL1 in real time. Migrating T cells form uropods at their rear, which are characterized by accumulation of F-actin (Pham et al., 2013). Indeed, migrating DN3a cells formed uropods with accumulation of F-actin at the rear of the migrating cell. Once the DN3a cell docks onto OP9-DL1 cells, F-actin relocates to the front of the cell and stabilizes at the interface (Fig. 2 A and Video 1). These findings are similar to observations of F-actin polarization in the formation of an immunological synapse by mature T cells (Ryser et al., 1982). We assessed the stability of F-actin polarization at the interface between DN3a and OP9-DL1 cells in real time for 3–4 h. Our results showed that polarization of F-actin at the interface was stable for an average period of 83 min (minimum, 36 min; maximum, 144 min;  $n = 22$ ). In addition, DN3a cells that left the OP9-DL1 lost their F-actin polarization. These data support our fixed imaging data and provide evidence that DN3a cells form a stable immunological synapse interaction with OP9-DL1 stromal cells.

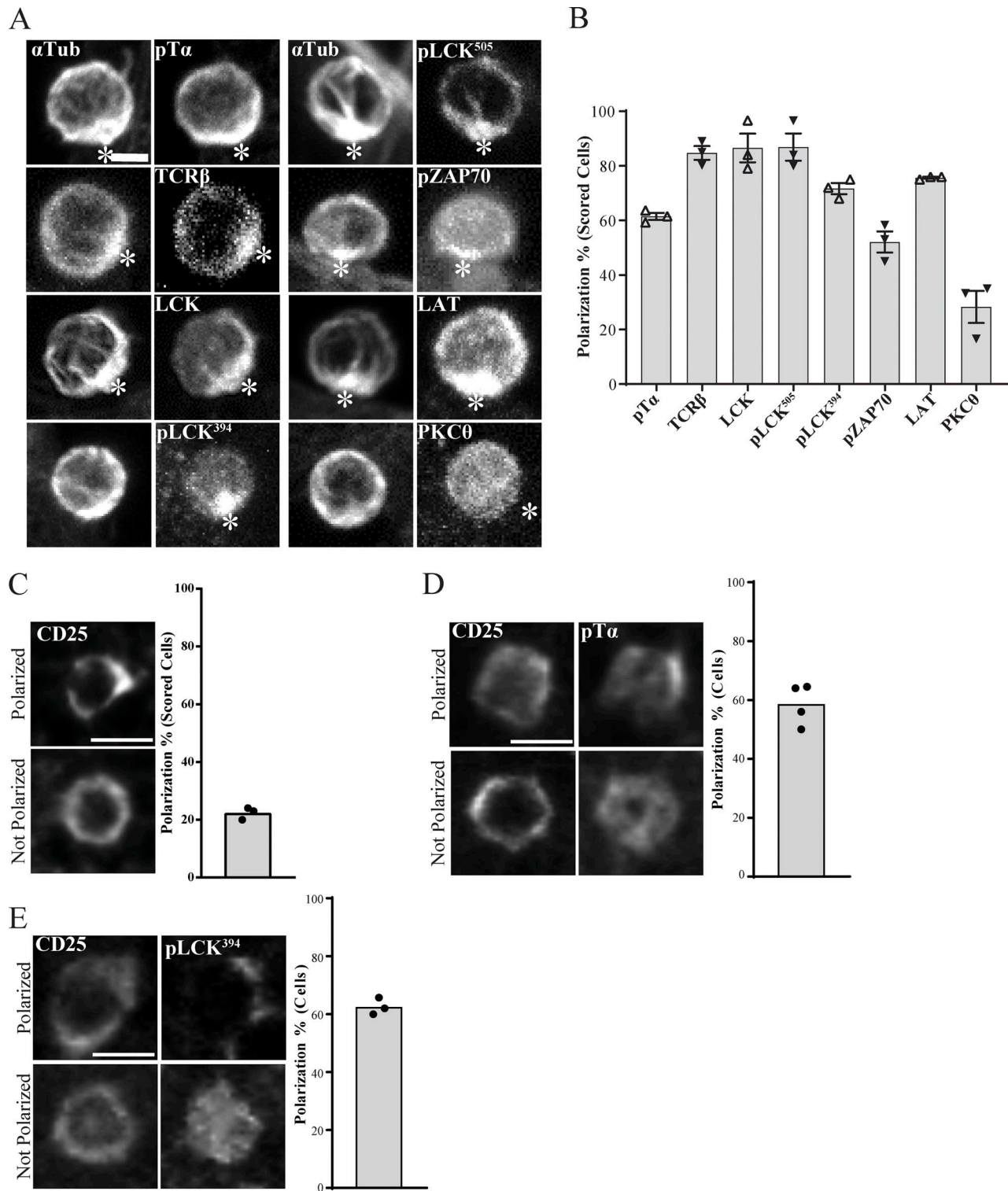


**Figure 1. Polarization of pre-TCR components in DN3 cells in vitro and in situ.** (A and B) DN3 cells were incubated with OP9-DL1 cells for 14 h and fixed and stained for  $\alpha$ -tubulin to mark the MTOC and a TCR-associated protein (as shown). Z-stack images were acquired using confocal microscopy, and representative images are shown as maximum projections (A). After triaging for cells in which the MTOC was recruited to the interface with an OP9-DL1 cell, the percentage of cells in which the TCR component was polarized to the interface (white asterisks) with the OP9-DL1 cell was determined by blind scoring (B). The total number of scored conjugates per marker is 75 (25 cells per biological replicate). (C) DN3 cells in a section of an intact thymus were stained for CD25 only as a nonpolarized control. (D and E) DN3 cells were stained for CD25 and either pT $\alpha$  (C) or pLCK<sup>394</sup>. Images were acquired using widefield fluorescent microscopy (Vectra 3 automated quantitative pathology imaging system), and representative images of polarized (top row) and nonpolarized (bottom row) are shown. Total number of scored cells:  $n = 156$  (pT $\alpha$ ) and  $n = 134$  (pLCK<sup>394</sup>). Scale bars represent 5  $\mu$ m (A) and 10  $\mu$ m (C–E). Error bars (B) represent SEM.

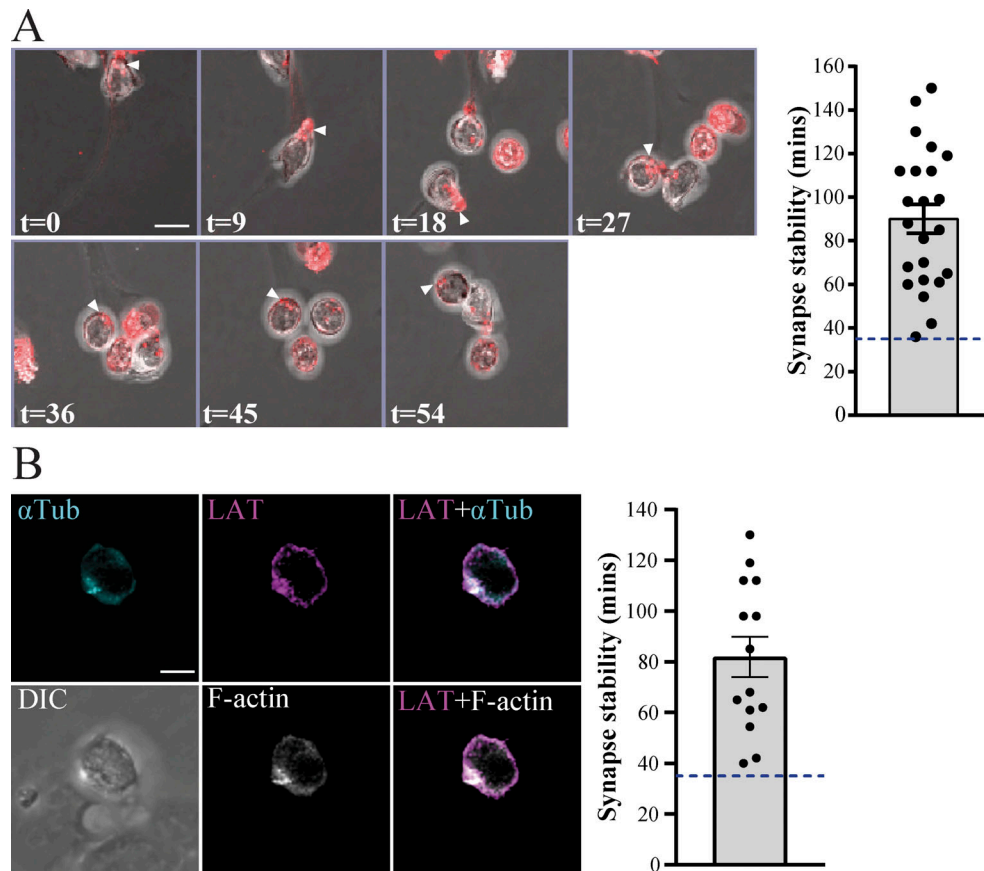


**Figure 2. DN3a cells form a stable immunological synapse. (A)** Sequential frames from time-lapse confocal microscopy of a DN3a cell docking onto OP9-DL1 cells (arrowheads indicate the cell of interest). F-actin (stained using SiR-F-actin dye) is shown in red and overlaid onto transmitted light images. Numbers on the bottom right of each panel indicate time in minutes. The entire movie is shown in [Video 1](#). The scatter plot represents the time for which actin polarization was maintained at the interface upon docking of DN3a cells onto OP9-DL1 (each data point represents a single cell, total  $n = 22$ ). **(B)** A single frame from time-lapse confocal microscopy of a DN3a cell docking onto OP9-DL1 (differential interference contrast [DIC]), showing polarization of  $\alpha$ -tubulin (cyan), LAT (magenta), and F-actin (white). The entire movie is shown in [Video 2](#). Scatter plot represents time periods in which  $\alpha$ -tubulin ( $\alpha$ Tub), LAT, and F-actin polarized at the interface between DN3a and OP9-DL1 (each data point represents a single cell, total  $n = 14$ ). Error bars (A and B) represent SEM.

To assess the relationship of this stable interaction with markers of an immunological synapse, we transduced developing T cell precursors with the T cell signaling protein LAT (GFP-tagged) and mCherry-tagged  $\alpha$ -tubulin to mark the MTOC. We sorted double-transduced DN3a cells and further stained for F-actin using SiR-Actin (Lukinavičius et al., 2014). We then co-cultured DN3a cells with OP9-DL1 stromal cells and used confocal microscopy to monitor the movement of these cells and the three fluorescent markers in real time. Upon DN3a docking onto OP9-DL1, LAT, MTOC, and F-actin are recruited to the interface and remained there for an average period of 82 min (minimum, 40 min; maximum, 130 min;  $n = 14$ ; [Fig. 2 B](#) and [Video 2](#)).

Thus, an immunological synapse containing activated pre-TCR signaling molecules is assembled upon docking of the DN3a cell onto stromal cells, can endure for over 1 h, and is present in T cells undergoing  $\beta$ -selection both in vitro and in situ. These findings suggest that an immunological synapse provides an alternative means of activating pre-TCR compared with the autonomous activation that has previously been proposed (Pang et al., 2010; Yamasaki and Saito, 2007). The findings also lend weight to an alternative proposal that pre-TCR

signaling can be facilitated by weak interactions with peptide-bound MHC (Mallis et al., 2015).

#### Notch1 and CXCR4 are required for immunological synapse formation in vitro and in situ

Given that the pre-TCR has only limited affinity for MHC-peptide complexes, we speculated that the recruitment of pre-TCR components to the interface with the stromal cell might depend upon other receptors. The fate determinant Notch1 and the chemokine receptor CXCR4 play essential roles in driving T cell development at the  $\beta$ -selection checkpoint (Maillard et al., 2006; Tramont et al., 2010; Charnley et al., 2019), cooperate with pre-TCR signaling (Garbe et al., 2006; Zhao et al., 2019), and are localized at the DN3-OPL-DL1 stromal cell interface (Pham et al., 2015; [Fig. S2](#)). Staining of DN3 cells conjugated to OP9-DL1 showed that pT $\alpha$  copolarized with Notch1 (68.4%) and CXCR4 (80%; [Fig. 3, A and B](#)). We investigated whether this copolarization could be observed in an intact mouse thymus using five-color immunofluorescence imaging. Almost all DN3 cells in the intact thymus were polarized for Notch1 and CXCR4, so we selected DN3 cells that were clustered for pT $\alpha$  and scored

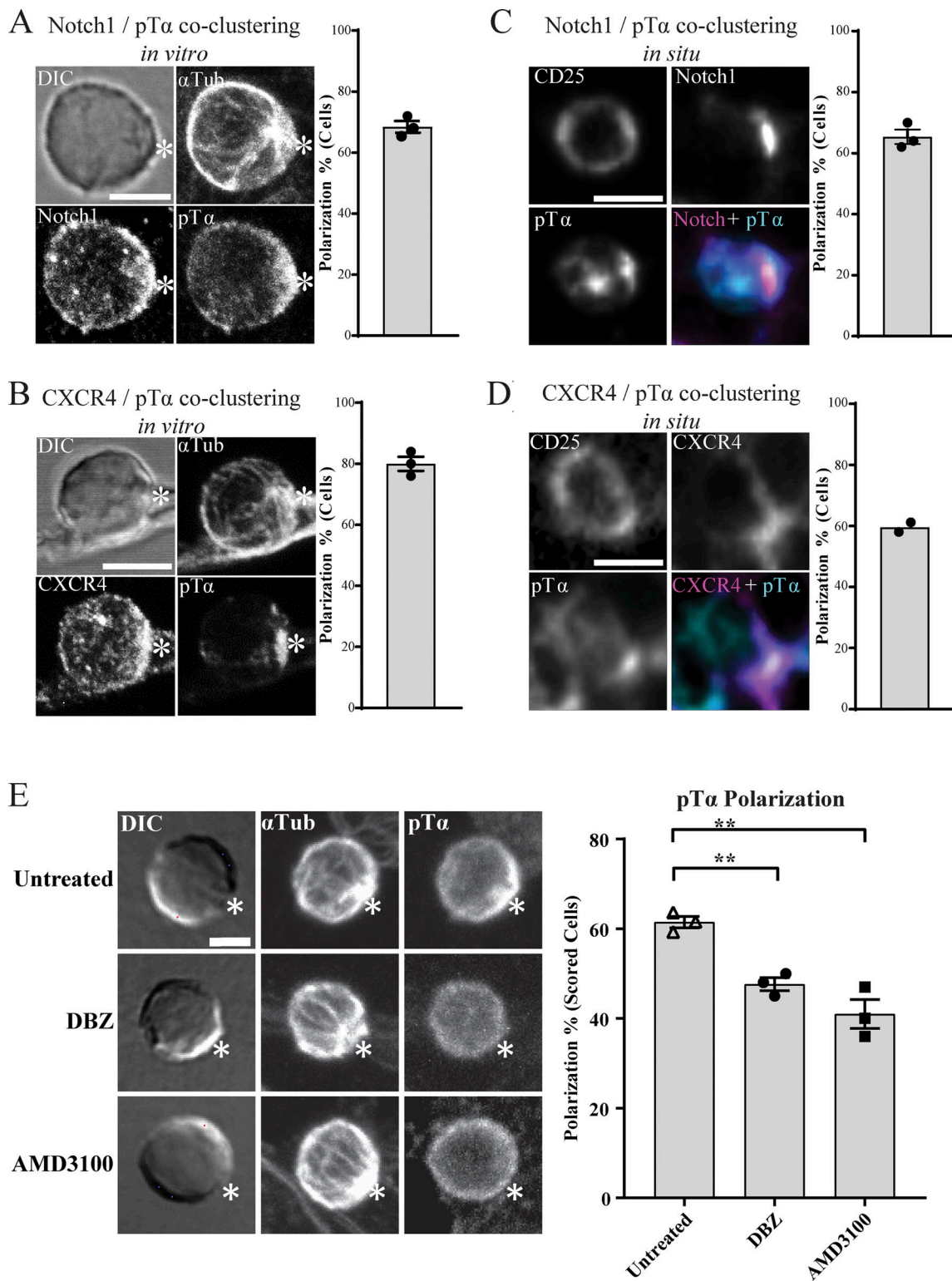


Figure 3. **Notch and CXCR4 recruit pre-TCR components to the stromal interface.** (A and B) DN3 cells were incubated with OP9-DL1 cells for 14 h and fixed and stained for  $\alpha$ -tubulin to mark the MTOC, Notch1, CXCR4, and pT $\alpha$  chain (as shown). Z-stack images were acquired using confocal microscopy, and representative images are shown as maximum projection. Asterisks indicate the interface between DN3 cells and OP9-DL1 cells. After triaging for cells in which the MTOC was recruited to the interface with an OP9-DL1 cell, the percentage of cells in which the pT $\alpha$  chain was polarized with either Notch1 or CXCR4 to the interface with the OP9-DL1 cell was determined by blind scoring. The total number of scored conjugates per marker is 75 (25 cells per biological replicate). (C and D) DN3 cells in an intact thymus were stained for CD25 as a nonpolarized control, pT $\alpha$  as a marker for pre-TCR, and either Notch1 (C) or CXCR4 (D). Images were acquired using widefield fluorescent microscopy (Vectra 3 automated quantitative pathology imaging system), and representative images of Notch1-pT $\alpha$  (C) and CXCR4-pT $\alpha$  (D) coclustering *in situ* are shown. The total number of scored cells is 150 (C) or 100 (D). (E) DN3 cells were incubated with OP9-DL1 cells for 14 h in the presence or absence of either Notch inhibitor (DBZ) or CXCR4 inhibitor (AMD3100) and then fixed and stained for  $\alpha$ -tubulin to

mark the MTOC and pT $\alpha$  chain as a marker of pre-TCR (as shown). After triaging for cells in which the MTOC was recruited to the interface with an OP9-DL1 cell, the percentage of cells in which pT $\alpha$  was polarized to the interface with the OP9-DL1 cell was determined by blind scoring (as shown by column-bar plot). The total number of scored conjugates per condition is 75 (25 cells per biological replicate). Scale bars represent 5  $\mu$ m (A and E) and 10  $\mu$ m (C and D). Statistics by one-way ANOVA test. Untreated vs. DBZ: \*\*,  $P = 0.019$ ; untreated vs. AMD3100: \*\*,  $P = 0.001$ . Error bars (A, B, C, D, and E) represent SEM.

for whether the pT $\alpha$  cluster colocalized with Notch1 and CXCR4. pT $\alpha$  was coclustered with Notch1 (65.3%) of these cells and with CXCR4 (59.5%; Fig. 3, C and D). These data indicate that Notch1 and CXCR4 assemble with the TCR signaling platform and raise the possibility that they facilitate the establishment of the immunological synapse.

The clustering of Notch1 and CXCR4 with pT $\alpha$  led us to suspect that Notch1 and CXCR4 might regulate pT $\alpha$  polarization. Indeed, scored DN3 conjugates treated for 14 h with pharmacological inhibitors of Notch signaling (dibenzazepine [DBZ]) or CXCR4 signaling (AMD3100) showed 47% and 41% pT $\alpha$  chain polarization, respectively, compared with 63.6% in the untreated sample (Fig. 3 E). We saw a similar reduction in pT $\alpha$  polarization after 3 h of signaling inhibition, suggesting that this effect is a direct rather than an indirect consequence of phenotypic changes induced by Notch or CXCR4 signaling (Fig. S3). These data suggest that Notch1 and CXCR4 act as recruiters of the pT $\alpha$  chain to the interface as a part of the de novo assembly of the immunological synapse.

#### The requirement for Notch1 and CXCR4 in passing the $\beta$ -selection checkpoint is circumvented by replacing the immunological synapse with pharmacological mimicry of TCR signaling

Both Notch and CXCR4 cooperate with pre-TCR signaling to facilitate progression beyond the  $\beta$ -selection checkpoint (Chann and Russell, 2019), but the mechanisms by which these signaling pathways interact is not known. We assessed whether the influence of Notch1 and CXCR4 signaling on  $\beta$ -selection might, at least in part, reflect their influence on the formation of the immunological synapse. It is well established that the  $\beta$ -selection checkpoint requires Notch1 and CXCR4 signaling (Ciofani et al., 2004; Janas et al., 2010; Maillard et al., 2006; Trampont et al., 2010; Yashiro-Ohtani et al., 2009), and we confirmed the impact of inhibiting Notch and CXCR4 signaling in the OP9-DL1 cocultures, where the survival of DN3a cells cocultured with the Notch inhibitor DBZ or the CXCR4 inhibitor AMD3100 was not affected, but fewer cells differentiated to DN3b and DP compared with the untreated coculture (Fig. 4 A). We assessed whether the impact of these inhibitors on differentiation correlates with an immediate downstream marker of pre-TCR signaling, pLCK<sup>394</sup>. 3 h after addition of Notch and CXCR4 inhibitors, pre-TCR signaling was reduced, as indicated by pLCK<sup>394</sup> levels (Fig. 4 B). The effectiveness of each inhibitor was confirmed by the reduction in expression of Hes1 and CXCR4 (readouts of Notch and CXCR4 signaling, respectively; Azab et al., 2009; Kageyama et al., 2007; Lee et al., 2013). Thus, the long-term impact on differentiation correlated with a short-term impact on pre-TCR signaling. In addition, these results support our previous findings that suggest that the impairment of pre-TCR clustering at the surface is due to Notch and CXCR4

inhibition. Indeed, our results are consistent with synapse disruption upon inhibition of pLCK<sup>394</sup> downstream TCR signaling in mature T cells (Tsun et al., 2011). In addition, the partial effect of each of the inhibitors is entirely consistent with the model that this signaling platform requires contributions from pre-TCR-MHC interactions, Notch, and CXCR4.

The above results demonstrate functional interactions among Notch1, CXCR4, and proximal pre-TCR signaling but do not indicate whether these interactions occur via assembly of the immunological synapse. To avoid confounding the results with cells that had already assembled an immunological synapse, we sorted DN3a cells for the presence or absence of surface TCR $\beta$ . As previously published, the cell surface expression of TCR $\beta$  dramatically alters subsequent fate of the cell populations (Klein et al., 2019). After 5 d of coculturing on OP9-DL1, TCR $\beta$ <sup>+</sup> cells yielded more than double the cells yielded by TCR $\beta$ <sup>-</sup> cells, with commensurate differences in CFSE dilution, indicating higher cell division rates (Fig. 5 A). TCR $\beta$ <sup>+</sup> cells produced increased numbers of DP cells compared with TCR $\beta$ <sup>-</sup> cells, and fewer DN3a cells remained in the culture (Fig. 5, B and C). In addition, Annexin V and propidium iodide (PI) staining showed that TCR $\beta$ <sup>+</sup> DN3a yielded fewer apoptotic and necrotic cells (Fig. 5 D). Thus, the presence and assembly of the pre-TCR is associated with increased differentiation and proliferation, and TCR $\beta$ <sup>-</sup> cells should represent TCR signaling-naïve cells appropriate for comparing pre-TCR signaling in the presence or absence of an immunological synapse.

To create a synapse-independent condition, we turned to a pharmacological mimic of TCR signaling, PMA, which bypasses the need for a signaling platform in mature T cells by directly activating PKC $\theta$  (Felli et al., 2005; Tahara et al., 2009). To compare synapse-dependent and synapse-independent responses to Notch and CXCR4 inhibition, we therefore sorted for TCR $\beta$ <sup>-</sup> DN3a cells (providing an initial population with no pre-assembled immunological synapse) and compared their differentiation in the presence (no PMA) or absence (with PMA) of an immunological synapse. A time course of response to incubation on OP9-DL1 cells revealed that TCR $\beta$ <sup>-</sup> DN3a cells remain viable and proliferate over 48 h (data not shown), but show very little progression through the differentiation stages, with most of the cells remaining as DN3a, suggestive of multiple cycles of self-renewal (Fig. 6 Ai, enumerated in Fig. 6 Aii). As expected, the addition of PMA caused differentiation through DN3b and DN4 (Fig. 6 A). Remarkably, Notch inhibition had no or a small inhibitory effect on differentiation from DN3a without PMA treatment but substantially increased differentiation from DN3a to DN3b and DN4 in the PMA-treated cells. The effects of Notch inhibition on differentiation were not related to cell death (Fig. S4 A). Inhibition of CXCR4 also showed a differential effect on differentiation in untreated versus PMA-treated cells, albeit to a lesser extent than inhibition of Notch (Fig. S4 B). These results

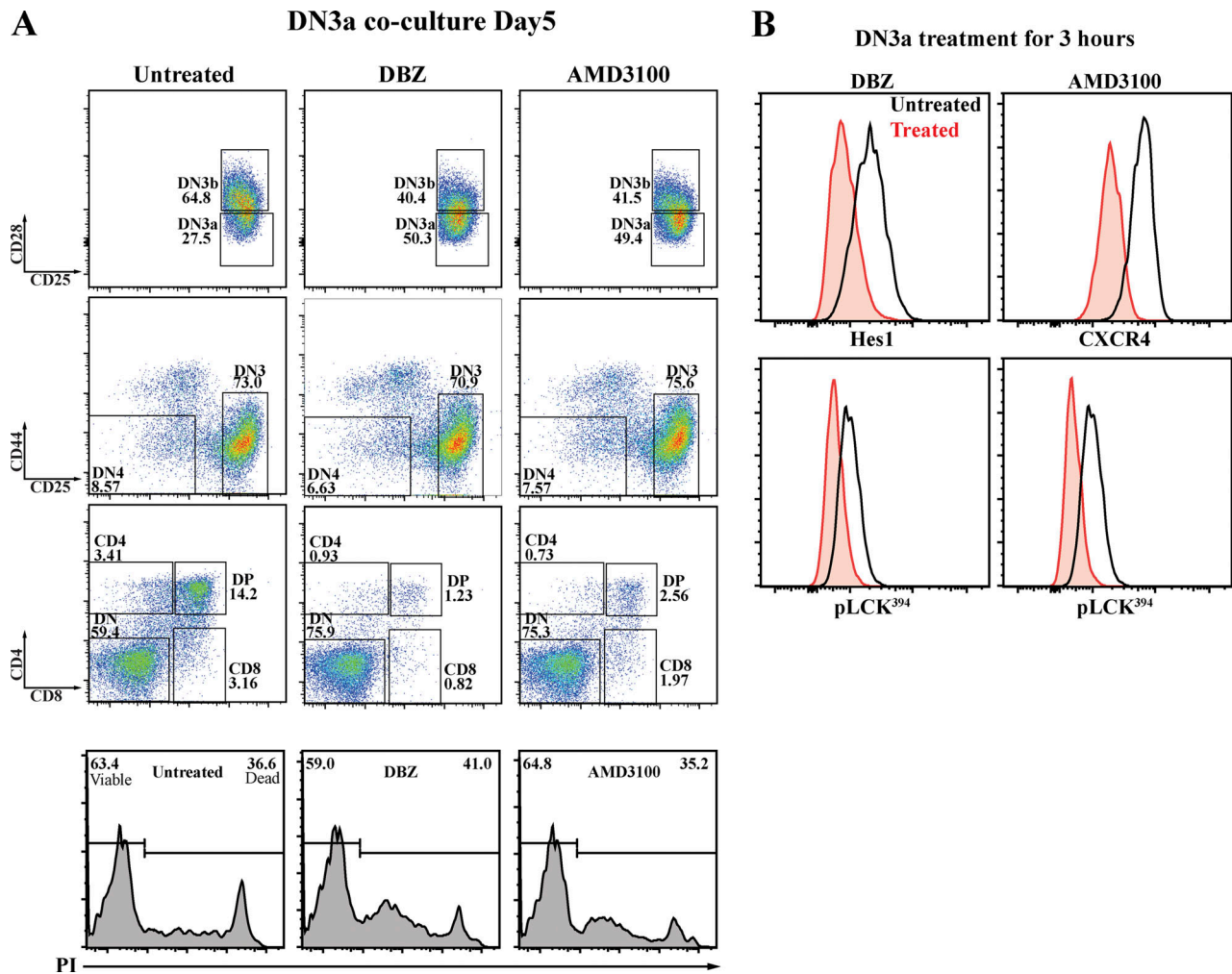


Figure 4. **Notch and CXCR4 signaling regulate the pre-TCR downstream signaling and are required for progression beyond  $\beta$ -selection.** (A) DN3a cells were cocultured with OP9-DL1 cells in the presence or absence of either Notch inhibitor (DBZ) or CXCR4 inhibitor (AMD3100). After 5 d, flow cytometry was used to assess the effect of Notch and CXCR4 inhibition on DN3a cell progression and differentiation. The effect of either Notch or CXCR4 inhibition on survival was assessed using PI intensities (as shown by bottom row histograms). (B) To assess the effect of Notch or CXCR4 inhibition on pre-TCR downstream signaling, purified DN3a cocultures were treated with either Notch inhibitor (DBZ) or CXCR4 inhibitor for 3 h and then fixed, and levels of pLCK<sup>394</sup> were assessed as a marker of pre-TCR downstream signaling (as shown by histograms). Hes1 and CXCR4 (top row) were stained to assess the effectiveness of inhibition of Notch and CXCR4, respectively. The results are representative of three independent biological replicates.

combined indicate that although both Notch and CXCR4 are required for differentiation in response to pre-TCR signaling, they are not required for differentiation in response to PMA signaling. Combined with our previous finding that Notch1 and CXCR4 are required for synapse formation and proximal TCR signaling, these results support the notion that rather than directly impacting upon differentiation, the major role for Notch1 and CXCR4 during  $\beta$ -selection is in de novo assembly of the immunological synapse.

**The coassembly of Notch1, CXCR4, and pre-TCR into a single signaling platform is correlated with progression through the  $\beta$ -selection checkpoint in situ**

It is well established that signaling through the pre-TCR during  $\beta$ -selection promotes cell proliferation (Miyazaki et al., 2008; Petrie et al., 2000). Therefore, we hypothesized that formation of the immunological synapse could be required for cell

proliferation after  $\beta$ -selection. Hence, we investigated the correlation between the coclustering of Notch1 and CXCR4 with pLCK<sup>394</sup> and proliferation of DN3 cells in situ. We established a six-color multiplex panel, where we validated the specificity of each used antibody by single staining (Fig. 7 A) and then used the HALO software region classifier module to distinguish among medullary, cortical, and subcapsular zones using the panel (Fig. 7 B). We focused on the subcapsular zone, where the DN3 cells reside (Love and Bhandoola, 2011), with Ki67 as a proliferation marker. Notch1 was coclustered with pLCK<sup>394</sup> in 63.3% of the scored cells in the subcapsular zone, where DN3 cells reside. Interestingly, 70.9% of the cells that showed copolarization of Notch1 and pLCK<sup>394</sup> in the subcapsular zone expressed Ki67 compared with 16.2% of these that did not show copolarization (Fig. 8, A and C). Similarly, CXCR4 was coclustered with pLCK<sup>394</sup> in 68% of the scored cells in the subcapsular zone. As with Notch1, 80.4% of the cells that showed copolarization of CXCR4

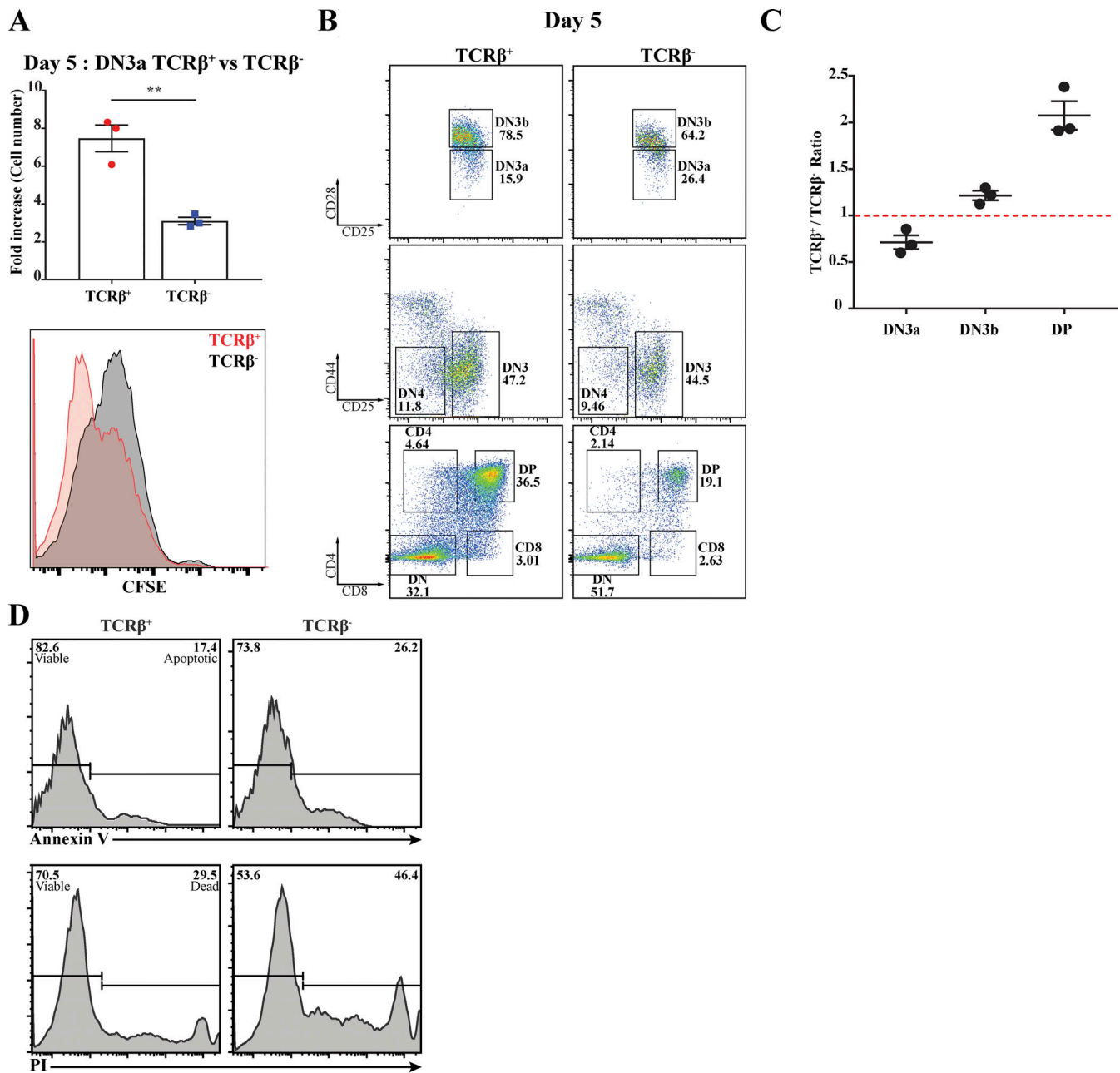


Figure 5. **Pre-TCR assembly at DN3a is critical for transition beyond the  $\beta$ -selection checkpoint.** Purified TCR $\beta^+$  and TCR $\beta^-$  DN3a cells were cocultured with OP9-DL1 for 5 d. **(A)** Cellularity was assessed by measuring fold increase in both cocultures (as shown in the column-bar plot), and proliferation was assessed using the intensity of CFSE (as shown in histogram, bottom left). **(B)** Flow cytometry was used to assess the differences between TCR $\beta^+$  and TCR $\beta^-$  DN3a cocultures progression and differentiation to subsequent developing stages (as shown by flow cytometry plots). **(C)** The percentages of DN3a, DN3b, and DP cells from three independent biological replicates were expressed as a ratio (TCR $\beta^+$ /TCR $\beta^-$ ) as shown by dot-plot (top right). **(D)** Purified TCR $\beta^+$  DN3a (indicates assembled pre-TCR) and TCR $\beta^-$  DN3a (lacks pre-TCR) cells were cocultured with OP9-DL1 for 5 d. Annexin V dye was used to assess apoptosis, and PI dye was used to assess cell death as shown by the histograms. The data are representative of three independent biological replicates with similar results. \*\*,  $P = 0.004$  (unpaired  $t$  test). Error bars (A and C) represent SEM.

and pLCK<sup>394</sup> in the subcapsular zone expressed Ki67 compared with 37.4% of these that did not show copolarization (Fig. 8, B and D). To be certain that Notch1 and CXCR4 copolarization with pLCK<sup>394</sup> is essential for proliferation and not due to pLCK<sup>394</sup> clustering, we scored cells that showed clustering of pLCK<sup>394</sup> only. Strikingly, pLCK<sup>394</sup> clustering did not correlate with Ki67 expression in the subcapsular zone (Fig. 8 E). These data strongly

support the hypothesis that Notch1 and CXCR4 are required for a proper assembly of the pre-TCR immunological synapse, which in turn propagates signaling via pLCK<sup>394</sup> to promote proliferation. These data together indicate that proliferation at the  $\beta$ -selection checkpoint is associated with formation of a signaling platform at the stromal interface, comprising Notch1, CXCR4, and the pre-TCR complex.



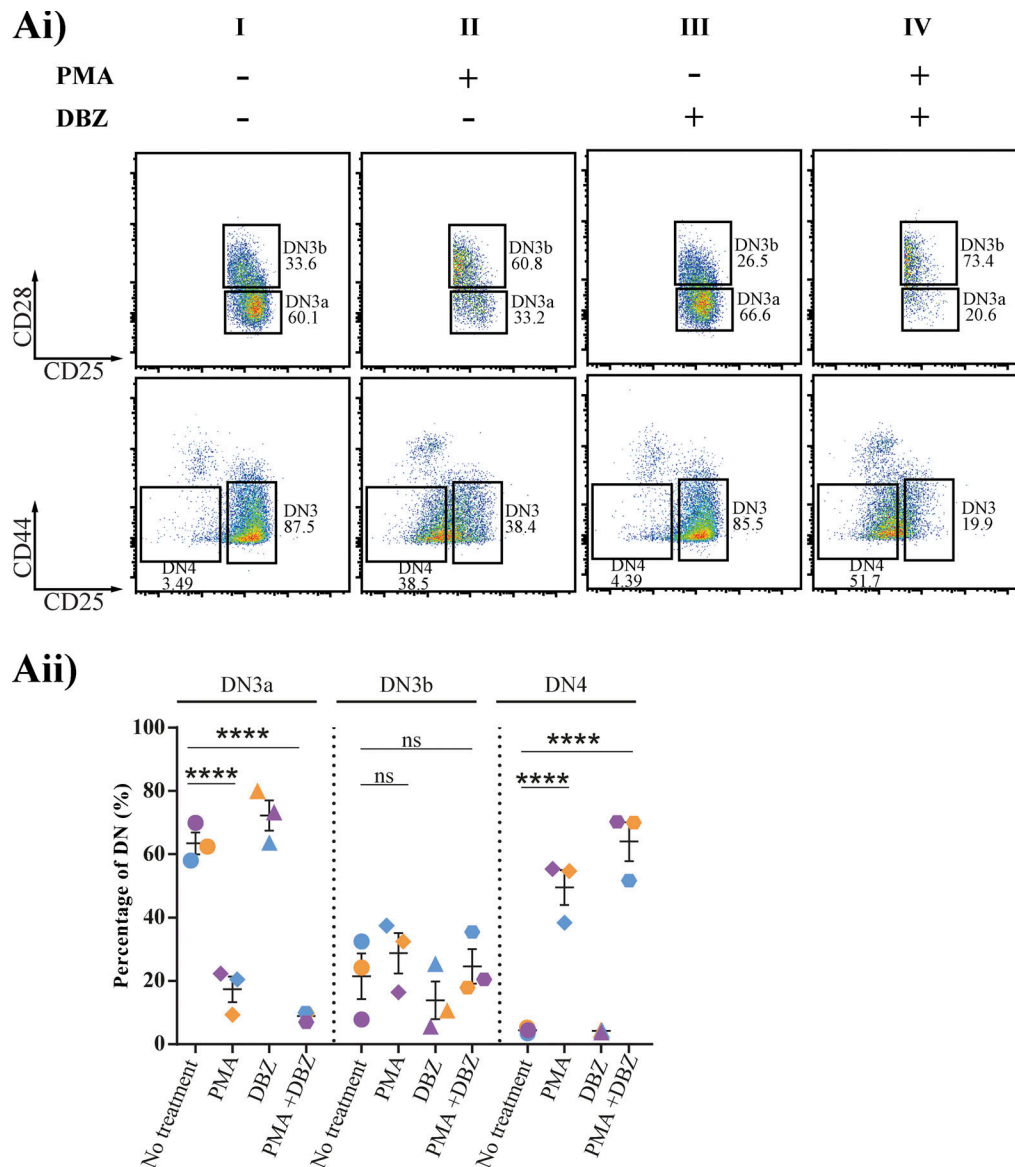


Figure 6. **The effect of inhibition of Notch signaling on progression beyond  $\beta$ -selection indicates a role in immunological synapse assembly. (Ai)** Purified TCR $\beta^-$  DN3a cells were cocultured on OP9-DL1 cells in the presence or absence of either of the following drug combinations: Notch inhibitor (DBZ), a pharmacological mimic of pre-TCR downstream signaling (PMA), and PMA with Notch inhibitor. Cocultures were stopped after 48 h and analyzed by flow cytometry to assess progression and differentiation (as shown by flow cytometry dot plots). **(Aii)** Scatter plot represents the percentages of DN3a, DN3b, and DN4 from three independent biological replicates (each experiment is color coded [purple, blue, and orange]) in the presence of PMA, DBZ, and PMA + DBZ. Flow cytometry plots are representative of three independent biological replicates. ns, not significant; \*\*\*\*,  $P < 0.0001$  (two-way ANOVA). Error bars (Aii) represent SEM.

### MHC plays a role in pT $\alpha$ chain clustering and the establishment of the pre-TCR immunological synapse

In mature T cells, the establishment of the immunological synapse is ligand dependent (Dustin et al., 2010). Although the pre-TCR signaling does not require interaction with ligand, it was shown recently that the pre-TCR can interact with peptide-MHC complexes to influence T cell development (Mallis et al., 2015). Therefore, we assessed whether a physical association of MHC and pre-TCR took place in an intact thymus. Using six-color immunofluorescent staining, we first assessed the proximity of DN3 cells to MHC class II (which we refer to as MHC)-expressing cells in intact thymic lobes. MHC showed patchy

staining consistent with it being variably expressed on the surface of some stromal cells. We made use of the variability in MHC expression to ascertain whether proximity to MHC correlated with pre-TCR clustering. We randomly picked five different regions of the same size the in thymic lobe (two thymic lobes from different mice, with a total of 322 scored cells) and scored cells for being either adjacent to or distant from MHC. We found that 52% of DN3 cells were adjacent to detectable MHC (Fig. 9 A). pT $\alpha$  was clustered in a higher proportion of DN3 cells adjacent to the MHC (87.8%) as compared with DN3 cells distant from the MHC (61.4%; Fig. 9 B). This finding is particularly striking given that the MHC might occur above or below the

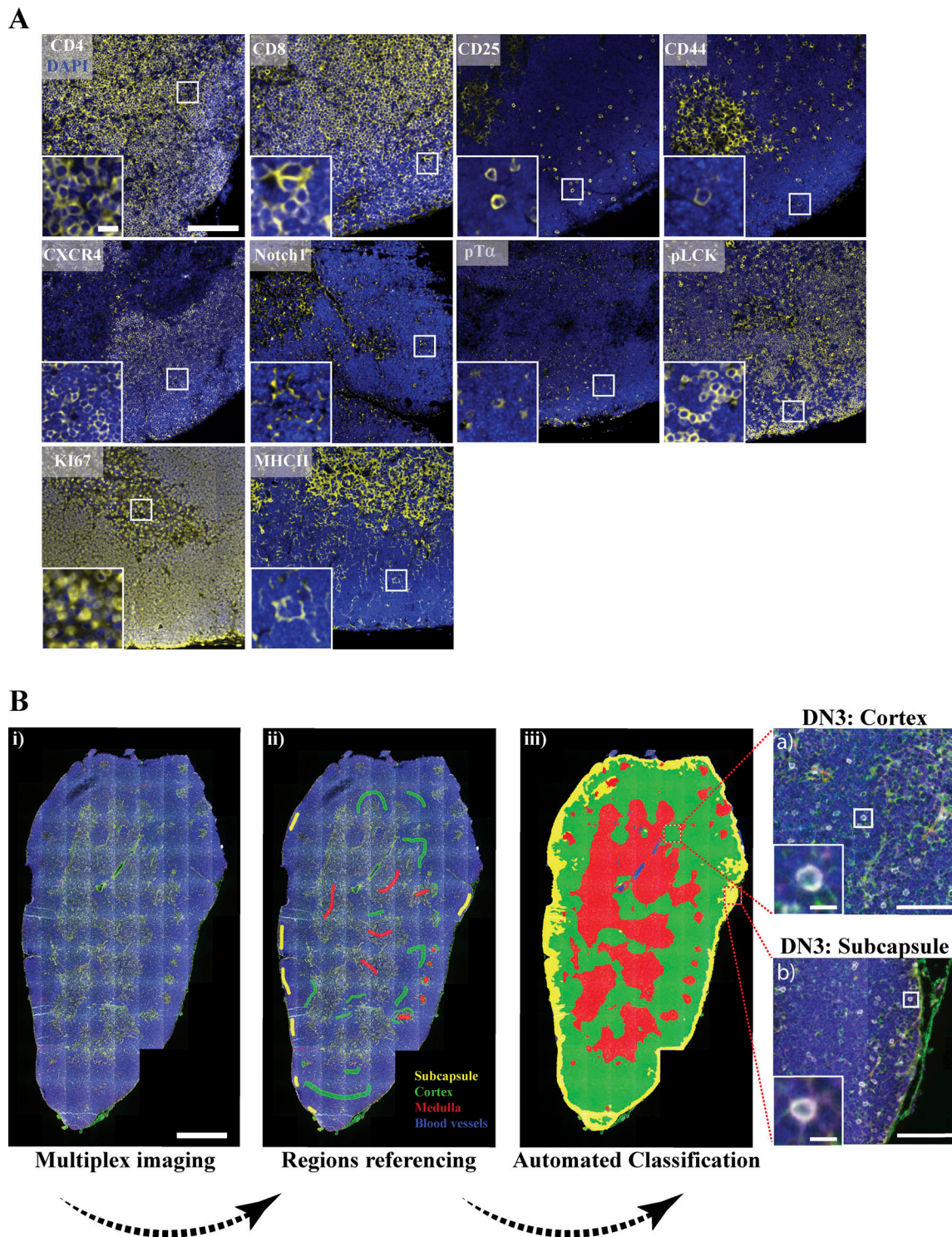


Figure 7. **Automated region classification of thymic lobes.** (A) A thymus lobe slice of 4  $\mu\text{m}$  thickness was stained and multiplex imaged using a 20 $\times$  air objective. Each marker of the multiplex thymus panel was stained with TSA dye (yellow), followed by DAPI staining to mark the nucleus (blue). Images were acquired using widefield fluorescent microscopy (Vectra 3 automated quantitative pathology imaging system), and representative images are shown. (B) Thymus lobes were stained with a six-color multiplex panel. Images were spectrally dissected and then stitched together using HALO Indica Laboratories software. Random regions of the subcapsular (yellow), cortical (green), and medullary (red) regions and blood vessels (blue) were marked as reference regions and stored in the software library (ii). An automated classification of entire tissue using reference regions library was performed (iii). Using CD4, CD8, CD44, and CD25 surface expression with regions classification, we could identify DN3 cells in the cortex (top zoomed image) or subcapsule (bottom zoomed image). Scale bars represent 50  $\mu\text{m}$  (A), 5  $\mu\text{m}$  (A, zoomed image), 1 mm (Bi), 100  $\mu\text{m}$  (Biii a and b, zoomed images) and 10  $\mu\text{m}$  (a and b, zoomed images).

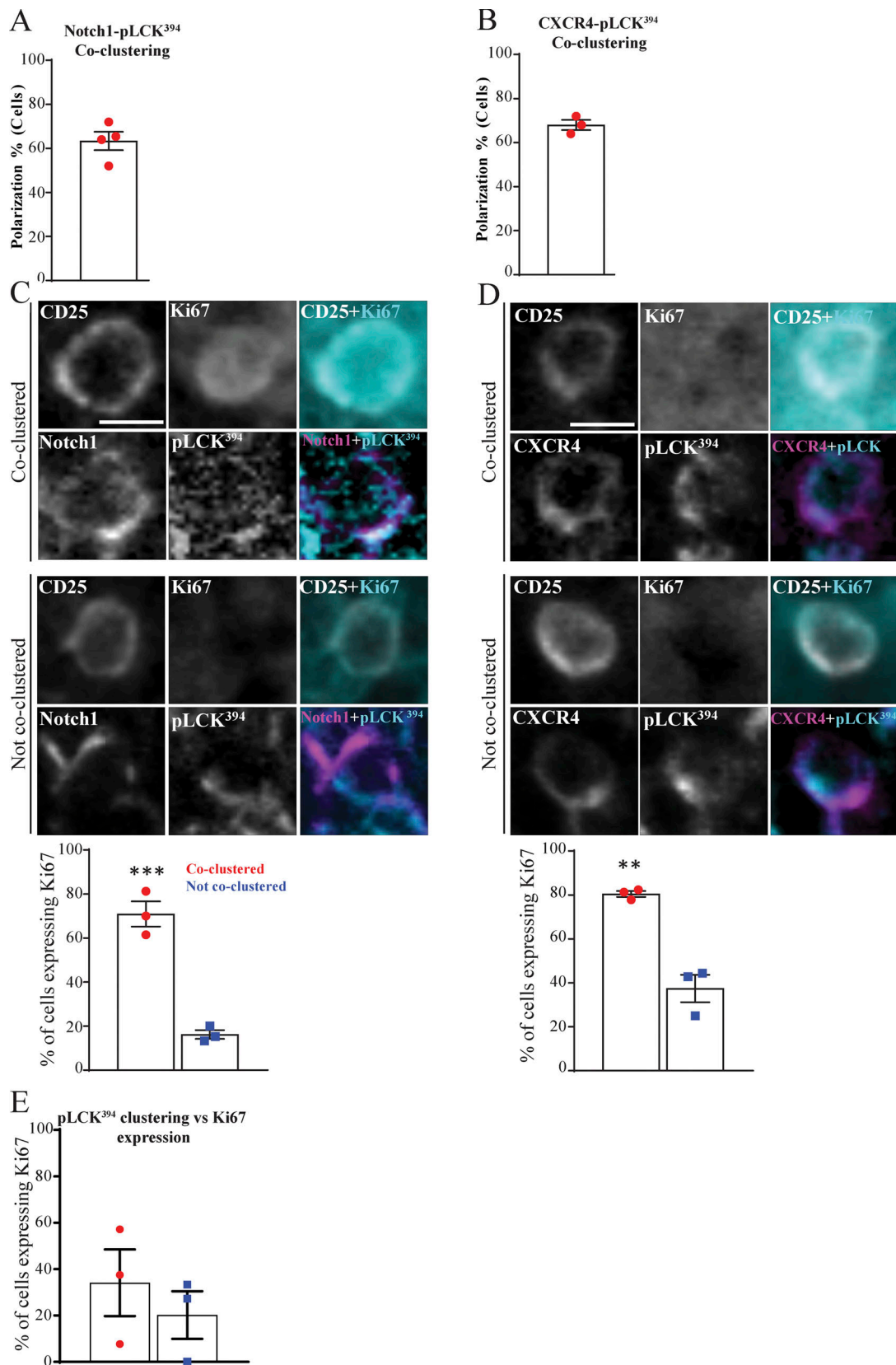


Figure 8. **The coassembly of Notch1, CXCR4, and pre-TCR into a single signaling platform is strongly associated with proliferation at the subcapsular zone in situ.** (A and B) Multiplex imaging on sections of an intact thymus was performed, followed by automated tissue classification using HALO software. DN3 cells in the subcapsular zone were identified and analyzed for CD25 as a nonpolarized control. The percentages of cells showed coclustering of pLCK<sup>394</sup> as a marker of pre-TCR signaling with either Notch1 (A) or CXCR4 (B) was determined as shown by the column-bar plots. The total number of scored cells is 100

(A) or 75 (B), with 25 cells per biological replicate. **(C and D)** DN3 cells were stained for CD25 as nonpolarizing control, pLCK<sup>394</sup> as marker for pre-TCR downstream signaling, Ki67 as a proliferation marker, and either Notch1 or CXCR4. Images were acquired using widefield fluorescent microscopy (Vectra 3 automated quantitative pathology imaging system), and representative images of highly expressed Ki67 when Notch1 (C) or CXCR4 (D) coclusters with pLCK<sup>394</sup> or a lack of Ki67 expression when Notch1 or CXCR4 does not cocluster with pLCK<sup>394</sup> in situ are shown. DN3 cells with coclustering or no coclustering of pLCK<sup>394</sup> with either Notch1 (C) or CXCR4 (D) in the subcapsular zone were assessed for levels of Ki67 expression, as shown by column-bar plots. The total number of scored cell is 75, with 25 cells per biological replicate. **(E)** DN3 cells in an intact thymic section were identified in the subcapsular zone, and the percentages of cells expressing the proliferation marker (Ki67) were assessed in cells showed clustering or no clustering of pLCK<sup>394</sup>, as shown by column-bar plots. The total number of scored cells is 75, with 25 cells per biological replicate. Scale bars, 10  $\mu\text{m}$ . \*\*,  $P = 0.0025$ ; \*\*\*,  $P = 0.0008$  (unpaired  $t$  test). Error bars (A, B, C, D, and E) represent SEM.

focal plane of imaging where it could not be detected, so not all cells in the 61.4% will be distant from the MHC. Moreover, of the DN3 cells adjacent to the MHC and with clustered pT $\alpha$ , the clustered pT $\alpha$  was oriented toward the MHC in 82.7% (Fig. 9 B). These data suggest that the pre-TCR can interact with the MHC in the intact thymus, supporting previous published work, suggesting that interactions with peptide-bound MHC fosters expansion of cells that can recognize self-MHC (Mallis et al., 2015). Moreover, these results suggest that MHC interactions are associated with the establishment of an immunological synapse during  $\beta$ -selection.

## Discussion

The  $\beta$ -selection checkpoint is the stage at which the developing T cell tests whether it has effectively recombined the gene for TCR $\beta$  (Bednarski and Sleckman, 2012; Rothenberg et al., 2008). Cells that fail this test will die, and cells that can signal through the pre-TCR downstream will pass the test and survive, proliferate, and differentiate (Kreslavsky et al., 2012; Michie and Zúñiga-Pflücker, 2002). In this study, we show that this test of pre-TCR signaling involves the establishment of an immunological synapse, resembling the immunological synapse of mature T cells (Fig. 10). The immunological synapse provides a platform for downstream signaling and progression beyond the  $\beta$ -selection checkpoint. Differing from that of mature T cells, the  $\beta$ -selection immunological synapse is facilitated by Notch1 and CXCR4 signaling.

The immunological synapse in a mature T cell is characterized by the polarization of the TCR components toward the antigen-presenting cell (Dustin et al., 2010; Martín-Cófreces et al., 2008; Mittelbrunn et al., 2011). In a similar manner, we find that the MTOC polarizes at the interface between DN3 and OP9-DL1 stromal cells (Pham et al., 2015), along with pre-TCR structural and signaling components such as Lck and LAT. Time-lapse imaging also indicates that cells stop moving for tens of minutes coincident with formation of the synapse, analogous to the slowing observed as mature T cells form an immunological synapse (Ludford-Menting et al., 2005) and the cessation of movement observed in more mature thymocytes undergoing negative selection (Le Borgne et al., 2009). Time-lapse imaging within an intact thymus will be required to test whether similar cessation of movement is observed in DN3a cells during  $\beta$ -selection in vivo. We also show polarization in situ in the intact thymus of both pT $\alpha$  (a component of the pre-TCR complex) and pLCK<sup>394</sup> (an indicator of signaling downstream of the pre-TCR). These results indicate that a signaling platform akin to

the well-characterized immunological synapse seen in mature T cells occurs during  $\beta$ -selection.

An intriguing aspect of the  $\beta$ -selection immunological synapse is the differences implied by incorporation of the pre-TCR rather than the  $\alpha\beta$  TCR. In the mature T cell immunological synapse, signaling and polarization are driven by TCR engagement with peptide-bound MHC (Fooksman et al., 2010). The possibility of the pre-TCR binding to peptide-bound MHC has only recently been indicated based upon interactions with purified proteins (Mallis et al., 2015). In support of a physiological relevance for binding to the MHC, the pre-TCR-MHC interaction was correlated with elevated levels of calcium influx, indicating active signaling (Das et al., 2016; Mallis et al., 2015). Although this interaction is clearly not essential for T cell development (Irving et al., 1998; Koller et al., 2010), Mallis and colleagues showed that it plays a critical role in encouraging the preferential proliferation of cells whose pre-TCR can bind self-MHC (Mallis et al., 2015). This is thought to skew the repertoire toward TCR $\beta$  repertoires before undergoing TCR $\alpha$  rearrangement (Mallis et al., 2015). Our findings that the MHC and pre-TCR cocluster toward each other suggest that the binding has functional relevance in the intact thymus. The formation of an immunological synapse also provides a potential mechanism for overcoming the weak binding between the pre-TCR and peptide-bound MHC, particularly before expression of the coreceptors CD4 and CD8. Together, these observations suggest that although the  $\beta$ -selection immunological synapse does not depend on peptide-bound MHC for its assembly, the synapse might promote pre-TCR signaling in response to peptide presented by adjacent thymic stromal cells.

Notch1 and CXCR4 are included in the  $\beta$ -selection immunological synapse in vitro and in situ, and their signaling is required for optimal assembly. These findings are compatible with our previous observations that Notch1 and CXCR4 polarize at the interface between the DN3 cell and OPL-DL1 (Pham et al., 2015). Others have identified a functional interaction between the pre-TCR and either Notch (Ciofani et al., 2004; Yashiro-Ohtani et al., 2009) or CXCR4 (Tramont et al., 2010) and that Notch and TCR are corecruited to the immunological synapse of mature T cells and DP (CD4<sup>+</sup>CD8<sup>+</sup>) thymocytes (Anderson et al., 2005; Guy et al., 2013). In mature T cells, TCR signaling enhances Notch recruitment to the immunological synapse (Guy et al., 2013). In contrast, our findings suggest that Notch and CXCR4 signaling are required for optimal assembly of a pre-TCR-containing immunological synapse. It is possible that the requirement for Notch and CXCR4 reflects compensation for the weaker binding of the pre-TCR to the MHC by creating a stable interface

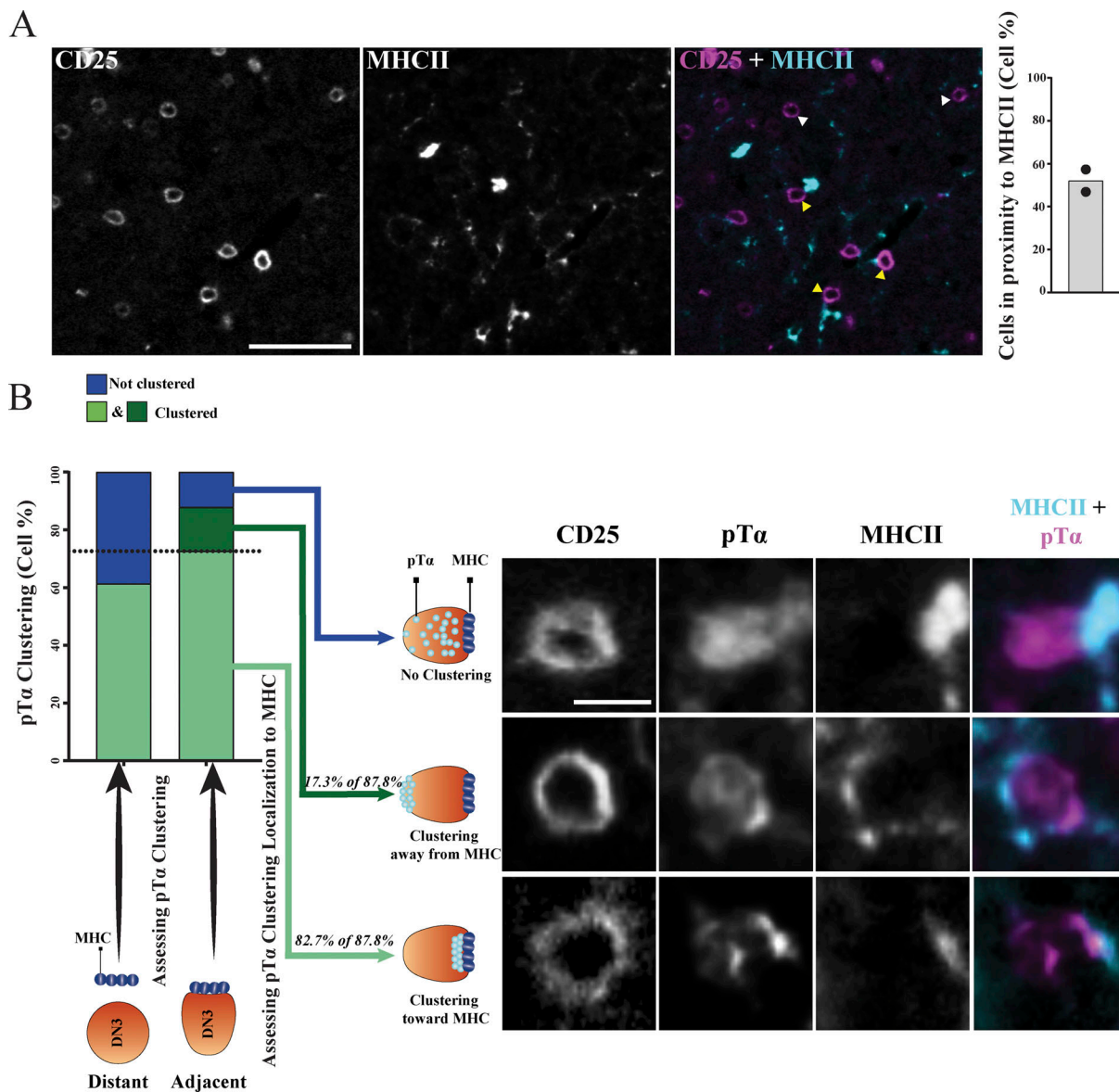


Figure 9. **MHC plays a role in establishing the pre-TCR immunological synapse at DN3 stage in situ.** (A) DN3 cells were identified in five randomly picked regions of the same size in an intact thymus to assess their localization in relationship to MHCII. Images were acquired using widefield fluorescent microscopy (Vectra 3 automated quantitative pathology imaging system) and are representative of DN3 cells adjacent (yellow arrowheads) or away (white arrowheads) from MHCII. DN3 cells were then scored as either adjacent to MHCII or away from it, as shown by the column-bar plot. The total number of scored cells is 322, with 161 per biological replicate. (B) pTα clustering was assessed in DN3 cells adjacent to or away from MHCII, as shown in the stacked column-bar plot. DN3 cells adjacent to MHCII that showed pTα clustering were assessed for the localization of pTα clustering as compared with MHCII, as shown by column-bar plot. Images were acquired using widefield fluorescent microscopy (Vectra 3 automated quantitative pathology imaging system), and representative images of DN3 cells adjacent to MHCII with clustering of pTα toward MHCII (I), clustering of pTα away from MHCII (II), and with no clustering of pTα (III) are shown. Scale bars represent 50 μm (A) and 10 μm (B).

between cells that allows for formation of the immunological synapse. These findings support the possibility that Notch and CXCR4 signaling initiate polarization and the MTOC (a key component of the immunological synapse) is recruited to the interface in response to both Notch and CXCR4 signaling.

These findings point to a possible alternative explanation for the cooperation among Notch, CXCR4, and pre-TCR at the β-selection checkpoint: in addition to (or instead of) cooperating at the level of downstream signaling, Notch and CXCR4 act to promote pre-TCR signaling by enabling the assembly of the

immunological synapse. To test this theory, we took advantage of a well-characterized surrogate for TCR signaling that does not involve assembly of an immunological synapse, PMA (Felli et al., 2005; Tahara et al., 2009). To compare PMA treatment with pre-TCR signaling, we established a system in which cells preferentially progressed either through the β-selection checkpoint via PMA signaling (DN3a cells that had not yet expressed the pre-TCR) or only via signaling through the pre-TCR (a mixed population of DN3a cells both expressing and not expressing TCRβ that were not treated with PMA). Consistent with recently published work (Klein

## Signaling Model

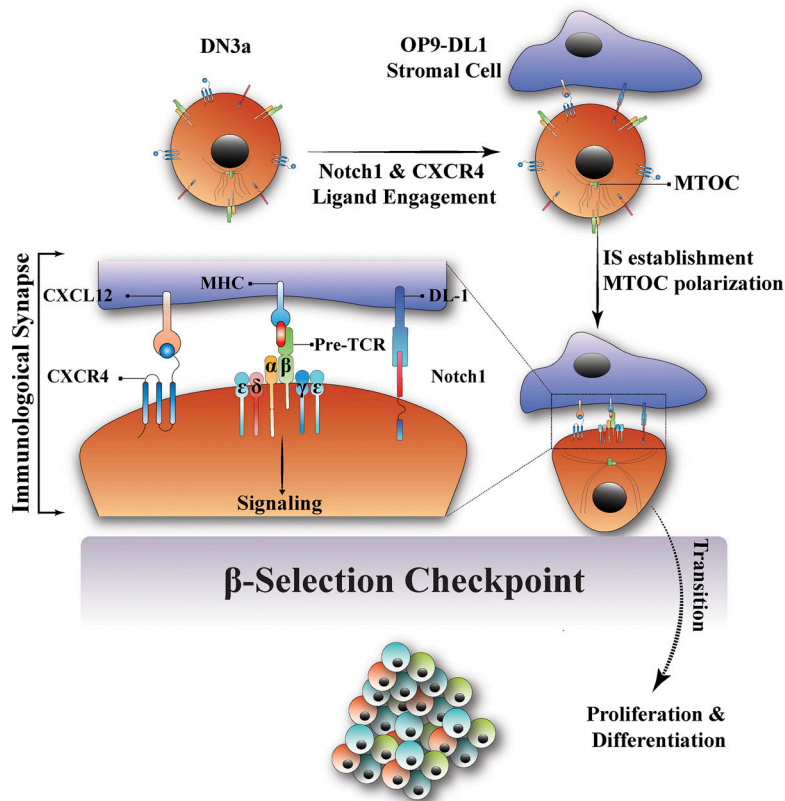


**Figure 10. A new model for the  $\beta$ -selection checkpoint that incorporates an immunological synapse.** In the proposed model, contact of DN3a developing T cells with stromal cells in the thymus (OP9-DL1 in vitro) causes Notch1 and CXCR4 to engage with their ligands (DL1/4 and CXCL12, respectively). Notch1 and CXCR4 engagement promotes the establishment of the immunological synapse via the pre-TCR (pT $\alpha$  and TCR $\beta$  chains). The immunological synapse is correlated with the polarization of MTOC, clustering of the CD3 complex (clustering of  $\epsilon$ ,  $\delta$ , and  $\gamma$  chains), and proximity to the MHC on the stromal cell. The immunological synapse then provides the signaling platform required for downstream signal transduction through the pre-TCR. Signaling via the pre-TCR promotes transition beyond the  $\beta$ -selection checkpoint, followed by proliferation and differentiation to the subsequent T cell developmental stages. IS, immunological synapse.

et al., 2019), DN3a cells that expressed cell surface TCR $\beta$  differentiated faster and proliferated more than those that did not express TCR $\beta$ , compatible with pre-TCR being a prerequisite for progression beyond the  $\beta$ -selection checkpoint. We used this system to discriminate between a role for Notch and CXCR4 in immunological synapse assembly compared with downstream signaling. The diametrically opposed responses of the two forms of pre-TCR signaling to inhibition of either Notch1 or CXCR4 suggest that at  $\beta$ -selection, the effects of Notch1 and CXCR4 on pre-TCR signaling act via the immunological synapse.

A hallmark of pre-TCR signaling is the onset of proliferation (Aifantis et al., 2001; von Boehmer, 2005). Accordingly, we tested whether the coclustering of Notch1 and CXCR4 with the pre-TCR downstream active signaling marker pLCK<sup>394</sup> correlated with proliferation of DN3 cells. Remarkably, our in situ multiplex imaging showed that coclustering of Notch1 and CXCR4 with pLCK<sup>394</sup> in DN3 thymocytes at the subscapular region had significantly higher expression of the proliferation marker Ki67 compared with those that showed no coclustering. This indicates that Notch1 and CXCR4 coclustering with pLCK<sup>394</sup> is critical for the proliferative expansion onset following pre-TCR signaling. Moreover, pLCK<sup>394</sup> clustering itself did not show a strong correlation with proliferation, which further supports the essential role of Notch1 and CXCR4 in establishing this signaling platform. Together, these findings suggest that assembly of the pre-TCR into an immunological synapse is a precondition for proliferation in response to  $\beta$ -selection.

In conclusion, we demonstrate the establishment of an immunological synapse that facilitates pre-TCR signaling during the  $\beta$ -selection checkpoint. We show that this immunological synapse is regulated cooperatively by Notch1 and CXCR4 signaling. We propose that the  $\beta$ -selection immunological synapse is critical for regulation of pre-TCR signaling and promotes progression beyond the  $\beta$ -selection stage.

## Materials and methods

### Primary hematopoietic coculture

The OP9 stromal cell line transduced to express the Notch ligand Delta-like1 (OP9-DL1; Schmitt and Zúñiga-Pflücker, 2002) was cultured in Minimal Essential Medium Alpha Modification (SAFC Biosciences, Sigma-Aldrich) supplemented with 10% (vol/vol) fetal calf serum, glutamine (1 mM; GIBCO-BRL), and 100 ng/ml penicillin/streptomycin at 37°C, 10% CO<sub>2</sub>. Fetal liver cells were extracted from embryonic day 14.5 C57 black 6 (C57BL/6) mice and used as hematopoietic stem cell progenitors. OP9-DL1 stromal cells were seeded in 6-well plates and mouse fetal liver cells were seeded onto them in a ratio 1:1 ( $2 \times 10^5$  cell/well). The coculture was maintained at 37°C, 10% CO<sub>2</sub> in Minimal Essential Medium Alpha Modification (SAFC Biosciences, Sigma-Aldrich) supplemented 10% fetal calf serum (vol/vol), glutamine (1mM),  $\beta$ -mercaptoethanol (50  $\mu$ M, Calbiochem), sodium pyruvate (1 nM; GIBCO-BRL), HEPES (10 mM; GIBCO-BRL), 100 ng/ml penicillin/streptomycin, 1 ng/ml mouse interleukin 7 (Peprotech),

and 5 ng/ml mouse FMS-like tyrosine kinase 3 (Peprotech). Upon hematopoietic confluency every 5–8 d, the coculture was harvested via pressure pipetting or gentle scrapping, and lymphocytes were separated from OP9-DL1 via pulse spin at 1,400 rpm and seeded onto fresh OP9-DL1 stromal cells in six-well plates. To investigate the effect of Notch1 and CXCR4 on the differentiation of purified DN3a, DN3a cells were purified by flow cytometric sorting, cocultured on OP9-DL1 stromal cells, and differentiation monitored in the presence and absence of Notch1 inhibitor (1 nM DBZ), CXCR4 inhibitor (2 µg/ml AMD3100), and the pharmacological mimic of TCR signaling, PMA (40 ng; Sigma-Aldrich).

### Flow cytometry sorting and analysis

All antibodies were purchased from eBioscience or BD Pharmingen unless otherwise specified. DN1–DN4, DP, and single positive thymocytes were distinguished using surface receptors, where DN1 (CD25<sup>-</sup>/CD44<sup>+</sup>/CD4<sup>-</sup>/CD8<sup>-</sup>), DN2 (CD25<sup>+</sup>/CD44<sup>hi</sup>/CD4<sup>-</sup>/CD8<sup>-</sup>), DN3 (CD25<sup>+</sup>/CD44<sup>lo</sup>/CD4<sup>-</sup>/CD8<sup>-</sup>), DN4 (CD25<sup>-</sup>/CD44<sup>hi</sup>/CD4<sup>-</sup>/CD8<sup>-</sup>), DP (CD4<sup>+</sup>/CD8<sup>+</sup>), and single positive (CD4<sup>+</sup>/CD8<sup>-</sup> or CD4<sup>-</sup>/CD8<sup>+</sup>). DN3a (early) and DN3b were discriminated using surface expression of CD28. We further discriminated late DN3a from early DN3b using TCRβ surface expression. Viability of cells was analyzed using FITC-Annexin V and/or PI. Refer to Table S1 for a list of all antibodies.

### Retroviral transductions

Phoenix cells were used to produce virus via transfection with 5 µg Murine Stem Cell Virus plasmid (pMSCV) retroviral constructs, mCherry-α-tubulin, and GFP-LAT using calcium phosphate transfection (courtesy of Mandy Ludford-Menting and Stephen Ting, Peter MacCallum Cancer Centre, Parkville, Victoria, Australia). Viral supernatant was collected 48 h after transfection virus and placed in a six-well plate (catalog no. 351146; Falcon, BD Pharmingen) that was precoated in 15 mg/ml RetroNectin/r-Fibronectin (Takara), blocked in 2% bovine serum albumin/phosphate buffer saline, and then spun at 2,000 *g* for 1 h. Six-well plates were incubated for 2 h at 37°C and 10% CO<sub>2</sub>. Supernatant was collected and discarded and thymocytes (day 8–10 culture) were added and spun down for 1 h at 1,200 *g*. Six-well plates were incubated overnight in culturing media at 37°C and 10% CO<sub>2</sub>. Thymocytes were collected and cultured onto OP9-DL1 cells in six-well plates. On days 14–15 of primary cocultures, flow cytometry was used to sort DN3a cells for live imaging.

### Confocal microscopy and immunofluorescence staining

OP9-DL1 stromal cells were seeded in each well of an 8-chamber slide (ThermoFisher) at 3 × 10<sup>3</sup> cell per well and incubated overnight at 37°C and 10% CO<sub>2</sub>. 4–5 × 10<sup>4</sup> hematopoietic precursors were seeded upon the OP9-DL1 stromal cells in each well with fresh media and then left in the incubator for 14 h. Cells were then fixed with 3.7% (wt/vol) paraformaldehyde in 100 mM Pipes, 5 mM MgSO<sub>4</sub>, 10 mM EGTA, and 2 mM DTT (20 min, RT), washed twice, and permeabilized in 0.1% Triton X-100 in PBS without MgCl<sub>2</sub> or CaCl<sub>2</sub> (7 min, RT), and then washed twice with PBS. All cells were blocked with 2% bovine serum albumin (30 min; Sigma-Aldrich) and washed twice with PBS;

primary antibody was added, and cells were left for 1 h at RT on a rocker. Cells were washed twice with PBS, secondary antibodies were added, cells were left for 1 h at RT on a rocker, and then cells were washed twice with PBS and mounted using Prolong Gold antifade (Molecular Probes). The slides were examined at room temperature using a FluoView FV1000 BX61 confocal microscope (Olympus) using a 40× 1.2 NA oil-immersion objective. 9–12 Z-stack images were acquired at a distance 1 µm per step, and then maximum intensity projections were generated using ImageJ software. Refer to Table S1 for a list of all antibodies.

For time-lapse imaging, F-actin was stained by incubating DN3a cells with SiR-Actin (1 µM; Cytoskeleton) for 2 h at 37°C and 10% CO<sub>2</sub>. SiR-Actin-labelled DN3a cells were seeded onto OP9-DL1 cells (3 × 10<sup>3</sup> of each cell type per chamber) in 35-mm glass-bottom four-chamber slides containing 250 µl culturing media. Multiple stage positions were acquired using confocal microscope (Olympus FV1000) using a 60× 1.3 NA oil objective every 2–4 min for up to 3 h with 10–12 z-stacks of 1 µm thickness. Cultures were imaged in a temperature-controlled unit at 37°C and 10% CO<sub>2</sub>. Acquired time lapses were processed using CellSens software.

### Formalin-fixed paraffin-embedded tissue samples and immunohistochemistry (IHC)

The thymi of 6-wk-old (C57BL/6) mice were extracted and washed in PBS and then fixed in 10% formaldehyde buffer for 18 h at RT. Fixed tissues were washed twice in PBS and then embedded in paraffin by a histologist. A serial section of 4 µm thickness was cut, and slices were mounted on glass slides. After deparaffinization, a heat antigen retrieval method using pressure cooker was used, and slides were placed in a plastic container filled with 1 mM EDTA (Sigma-Aldrich) antigen retrieval buffer solution at pH 9.0. To validate the specificity and detection of primary antibodies, chromogenic IHC was performed for each single antibody as follows; slides were blocked using 2% BSA for 1 h at RT on a rocker. Primary antibodies were incubated for 1 h at RT on a rocker and then washed twice with 1×Tris-buffered saline 0.5% Tween (TBST; 1 mM Tris Base, 1.8% NaCl, and 0.5% Tween 20, pH 7.4). Endogenous peroxidase was blocked by incubating the slides in 0.3% hydrogen peroxidase for 10 min at RT, followed by washing twice in 1×TBST. HRP-conjugated secondary antibodies (Vector Labs) was added for 1 h at RT on a rocker, and then slides were washed twice with 1×TBST. Slides were incubated with a 3,3'-DAB chromogen kit (DAKO) for 10 min at RT on a rocker and then washed twice with 1×TBST. Samples were counterstained with hematoxylin and dehydrated with ethanol and xylene to prepare for mounting. Slides were scanned using 20× air objective on Olympus V120 slide scanner (Fig. 5). The antibodies were used to build a thymic multiplex antibodies panel (Table S2).

### Opal multiplex immunofluorescence imaging of thymic sections

#### Uniplex immunofluorescence validation

Following chromogenic detection, each of the assessed antibodies was further titrated for Opal multiplex imaging. Monocolor staining of each of the antibodies was performed using the

Opal seven-color kit (PerkinElmer) following the same protocol used for IHC; after incubation with the HRP-conjugated secondary antibodies, slides were incubated with individual tyramide signal amplification (TSA)-conjugated fluorophores for 5–10 min at RT on a rocker and then washed three times with 1×TBST. Slides were then mounted with Citifluor Poly (vinyl pyrrolidone) plus antifadent solution (Citifluor) and scanned at RT using a 20× objective on the Vectra 3 automated quantitative pathology imaging system (PerkinElmer; Fig. S5). Acquired images were used to build spectral library of all the target proteins using in Form Cell Analysis software (PerkinElmer).

### Multiplex imaging

Following validating target antibodies and building the spectral library described in the paragraph above, multiplex staining was performed by following the same steps for uniplex staining. After adding the first TSA dye, the slides were placed in plastic container and microwaved for 1 min at 100°C and then microwaved for 10 min at 75°C to remove the primary and secondary antibodies, leaving behind the TSA dye. The same steps were then performed with each subsequent antibody up to a maximum of seven antibodies. After the last antibody, slides were incubated with DAPI (1:1,000 in 1×TBST) stain (Spectral DAPI; PerkinElmer) for 2–3 min at RT on a rocker and then washed twice with 1×TBST. Slides were then mounted using Citifluor Poly (vinyl pyrrolidone) plus antifadent solution, and the entire tissue was imaged using a 20× objective on the Vectra 3 automated quantitative pathology imaging system.

### inForm and HALO software

Acquired images were loaded to inForm cell analysis software, and the spectral library built from uniplex staining of the target antibodies was used to spectrally dissect multiplex images. Images were then exported as component .tiff files. Component .tiff files were then uploaded to HALO image analysis software (Indica Labs) and fused to build the thymic lobe. Using the HALO Highplex FL region classifier module, the software was trained to distinguish three main regions in the thymus (medulla, cortex, and subcapsular region) by manually picking 5–10 regions for each and then running automated classification on the entire tissue to highlight these three regions (Fig. 7). DN3 cells were identified either in the cortex or subcapsular zone using CD25<sup>+</sup> CD44<sup>-</sup> CD4<sup>-</sup> CD8<sup>-</sup> surface expression.

### Clustering and colocalization quantification

#### In vitro scoring and cell triaging

One of the hallmarks of the immunological synapse formation in mature T cells is the polarization of the MTOC to the interface (Martín-Cófreces et al., 2008). Accordingly, we first identified cell conjugates in vitro by relying on the polarization of the MTOC to the interface with OP9-DL1 stromal cells. We took into consideration that the MTOC and OP9-DL1 should be on the same focal plane and only selected conjugates with visible fluorescence for the marker of interest. It should be noted that almost all of the markers in this study showed clusters. We scored for single marker clustering, where clustering at the interface was given a score of 1 and no clustering was given a score

of 0. For double-marker scoring, we scored for conjugates showing visible fluorescence intensity of both markers at the same focal plane. We scored for the colocalization of both marker clusters at the interface, where colocalized clusters at the interface were given a score of 1 and no colocalization at the interface was given a score of 0.

#### In situ scoring and cell triaging

Due to the technical difficulty of using MTOC polarization as a guideline to identify conjugates in our in situ system, we only scored for clustering and colocalizations of clustered markers of interest. First, DN3 cells were identified either in the cortex or subcapsular zone using CD25<sup>+</sup> CD44<sup>-</sup> CD4<sup>-</sup> CD8<sup>-</sup> surface expression. For single-marker clustering, we only scored cells with visible fluorescence intensity of the marker of interest and in focus. These cells were scored as 1 when they were clearly clustered, cells that showed clustering were given a score of 1, and no clustering was given a score of 0. When comparing the clustering of more than one marker, we scored cells with visible fluorescence intensity of both markers and in focus. We used the following strategy to avoid confounding the results with colocalization of nonclustered protein: since almost all cells in situ showed clustering of Notch1 (100% of cells) and CXCR4 (80–88% of cells) but fewer cells showed clustering of pTα (53%) and pLCK<sup>394</sup> (61%), we only scored cells that showed clustering of pTα and pLCK<sup>394</sup>. We then scored the clustered markers for colocalization, where colocalized clusters were scored as 1 and noncolocalized clusters were scored as 0.

#### Statistics

All data from flow cytometry, immunofluorescence staining, and time-lapse microscopy were assumed to have normal distributions. Unpaired Student's *t* tests and one- or two-way ANOVA tests were performed depending on the experiment.

#### Online supplemental material

Fig. S1 shows that DN3a cells express pre-TCR structural and signaling molecules. Fig. S2 shows that Notch1 and CXCR4 polarize at the interface between DN3a and OP9-DL-1 in vitro. Fig. S3 shows that inhibition of Notch1 and CXCR4 for 3 h disrupts pTα chain polarization. Fig. S4 shows that inhibition of CXCR4 promotes defective progression of TCRβ<sup>-</sup> DN3a cells beyond β-selection, indicating a role in immunological synapse assembly. Fig. S5 illustrates chromogenic detection of the markers used in establishing the six-color multiplex panel. Video 1 shows that F-actin polarizes and stabilizes at the interface between DN3a and OP9-DL1, indicating the establishment of an immunological synapse. Video 2 shows MTOC, F-actin, and LAT polarization at the interface between DN3a and OP9-DL1, indicating the establishment of an immunological synapse. Table S1 lists antibodies used in flow cytometry and immunofluorescence. Table S2 describes the antibodies used in the thymus multiplex antibodies panel.

### Acknowledgments

We thank Helena Richardson (La Trobe University) and Joe Trapani (Peter MacCallum Cancer Centre) for comments on the



manuscript. This work was performed in part at the Biointerface Engineering Hub at Swinburne, part of the Victorian node of the Australian National Fabrication Facility, a company established under the National Collaborative Research Infrastructure Strategy to provide nano- and microfabrication facilities for Australia's researchers. This work was done on Wurundjeri land of the Kulin nation, and we pay our respects to the Elders past and present.

Multiplexed IHC was supported by the Centre for Advanced Histology and Microscopy at the Peter MacCallum Cancer Centre, and the flow cytometry was enabled by support from the L.E.W. Carty Charitable Fund. This work was funded by the Australian Research Council (grant FT0990405 to S.M. Russell), the National Health and Medical Research Council (grant APP1099140 to S.M. Russell), the Schweizerischer Nationalfonds zur Förderung der Wissenschaftlichen Forschung (Swiss National Science Foundation; grants PA00P3\_142120 and P300P3\_154664 to M. Charnley), and a Swinburne University Postgraduate Research Award to A.H. Allam.

The authors declare no competing financial interests.

Author contributions: A.H. Allam contributed to conceptualization, data curation, formal analysis, investigation, methodology, validation, visualization, writing, reviewing, and editing; M. Charnley contributed to conceptualization, project administration, supervision, and review and editing of the manuscript; K. Pham contributed to conceptualization and review and editing of the manuscript; and S.M. Russell contributed to conceptualization, formal analysis, funding acquisition, methodology, project administration, supervision, visualization, and writing, review, and editing of the manuscript.

Submitted: 12 August 2019

Revised: 22 October 2020

Accepted: 10 December 2020

## References

Aifantis, I., F. Gounari, L. Scorrano, C. Borowski, and H. von Boehmer. 2001. Constitutive pre-TCR signaling promotes differentiation through Ca<sup>2+</sup> mobilization and activation of NF- $\kappa$ B and NFAT. *Nat. Immunol.* 2: 403–409. <https://doi.org/10.1038/87704>

Aifantis, I., C. Borowski, F. Gounari, H.D. Lacorazza, J. Nikolich-Zugich, and H. von Boehmer. 2002. A critical role for the cytoplasmic tail of pTalpha in T lymphocyte development. *Nat. Immunol.* 3:483–488. <https://doi.org/10.1038/ni779>

Alarcón, B., D. Mestre, and N. Martínez-Martín. 2011. The immunological synapse: a cause or consequence of T-cell receptor triggering? *Immunology.* 133:420–425. <https://doi.org/10.1111/j.1365-2567.2011.03458.x>

Alcover, A., V. Di Bartolo, and P. Roda-Navarro. 2016. Editorial: Molecular Dynamics at the Immunological Synapse. *Front. Immunol.* 7:632. <https://doi.org/10.3389/fimmu.2016.00632>

Anderson, A.C., E.A. Kitchens, S.W. Chan, C. St Hill, Y.N. Jan, W. Zhong, and E.A. Robey. 2005. The Notch regulator Numb links the Notch and TCR signaling pathways. *J. Immunol.* 174:890–897. <https://doi.org/10.4049/jimmunol.174.2.890>

Azab, A.K., J.M. Runnels, C. Pittsillides, A.-S. Moreau, F. Azab, X. Leleu, X. Jia, R. Wright, B. Ospina, A.L. Carlson, et al. 2009. CXCR4 inhibitor AMD3100 disrupts the interaction of multiple myeloma cells with the bone marrow microenvironment and enhances their sensitivity to therapy. *Blood.* 113: 4341–4351. <https://doi.org/10.1182/blood-2008-10-186668>

Bednarski, J.J., and B.P. Sleckman. 2012. Lymphocyte development: integration of DNA damage response signaling. *Adv. Immunol.* 116:175–204. <https://doi.org/10.1016/B978-0-12-394300-2.00006-5>

Carpenter, A.C., and R. Bosselut. 2010. Decision checkpoints in the thymus. *Nat. Immunol.* 11:666–673. <https://doi.org/10.1038/ni.1887>

Chann, A.S., and S.M. Russell. 2019. An integrated transcriptional switch at the  $\beta$ -selection checkpoint determines T cell survival, development and leukaemogenesis. *Biochem. Soc. Trans.* 47:1077–1089. <https://doi.org/10.1042/BST20180414>

Charnley, M., M. Ludford-Menting, K. Pham, and S.M. Russell. 2019. A new role for Notch in the control of polarity and asymmetric cell division of developing T cells. *J. Cell Sci.* 133:jcs235358. <https://doi.org/10.1242/jcs.235358>

Ciofani, M., T.M. Schmitt, A. Ciofani, A.M. Michie, N. Cuburu, A. Aublin, J.L. Maryanski, and J.C. Zúñiga-Pflücker. 2004. Obligatory role for cooperative signaling by pre-TCR and Notch during thymocyte differentiation. *J. Immunol.* 172:5230–5239. <https://doi.org/10.4049/jimmunol.172.9.5230>

Das, D.K., R.J. Mallis, J.S. Duke-Cohan, R.E. Hussey, P.W. Tetteh, M. Hilton, G. Wagner, M.J. Lang, and E.L. Reinherz. 2016. Pre-T Cell Receptors (Pre-TCRs) Leverage V $\beta$  Complementarity Determining Regions (CDRs) and Hydrophobic Patch in Mechanosensing Thymic Self-ligands. *J. Biol. Chem.* 291:25292–25305. <https://doi.org/10.1074/jbc.M116.752865>

Dustin, M.L., and C.T. Baldari. 2017. The immune synapse: past, present, and future. In *The Immune Synapse: Methods and Protocols*. C.T. Baldari and M.L. Dustin, editors. Springer, New York. 1–5. [https://doi.org/10.1007/978-1-4939-6881-7\\_1](https://doi.org/10.1007/978-1-4939-6881-7_1)

Dustin, M.L., A.K. Chakraborty, and A.S. Shaw. 2010. Understanding the structure and function of the immunological synapse. *Cold Spring Harb. Perspect. Biol.* 2:a002311. <https://doi.org/10.1101/cshperspect.a002311>

Felli, M.P., A. Vacca, A. Calce, D. Bellavia, A.F. Campese, R. Grillo, M. Di Giovine, S. Checquolo, C. Talora, R. Palermo, et al. 2005. PKC $\theta$  mediates pre-TCR signaling and contributes to Notch3-induced T-cell leukemia. *Oncogene.* 24:992–1000. <https://doi.org/10.1038/sj.onc.1208302>

Fooksman, D.R., S. Vardhana, G. Vasiliver-Shamis, J. Liese, D.A. Blair, J. Waite, C. Sacristán, G.D. Victoria, A. Zanin-Zhorov, and M.L. Dustin. 2010. Functional anatomy of T cell activation and synapse formation. *Annu. Rev. Immunol.* 28:79–105. <https://doi.org/10.1146/annurev-immunol-030409-101308>

Garbe, A.I., A. Krueger, F. Gounari, J.C. Zúñiga-Pflücker, and H. von Boehmer. 2006. Differential synergy of Notch and T cell receptor signaling determines alphabeta versus gammadelta lineage fate. *J. Exp. Med.* 203:1579–1590. <https://doi.org/10.1084/jem.20060474>

Gascoigne, N.R., V. Rybakin, O. Acuto, and J. Brzostek. 2016. TCR Signal Strength and T Cell Development. *Annu. Rev. Cell Dev. Biol.* 32:327–348. <https://doi.org/10.1146/annurev-cellbio-111315-125324>

Gaud, G., R. Lesourne, and P.E. Love. 2018. Regulatory mechanisms in T cell receptor signalling. *Nat. Rev. Immunol.* 18:485–497. <https://doi.org/10.1038/s41577-018-0020-8>

Groettrup, M., K. Ungewiss, O. Azogui, R. Palacios, M.J. Owen, A.C. Hayday, and H. von Boehmer. 1993. A novel disulfide-linked heterodimer on pre-T cells consists of the T cell receptor beta chain and a 33 kd glycoprotein. *Cell.* 75:283–294. [https://doi.org/10.1016/0092-8674\(93\)80070-U](https://doi.org/10.1016/0092-8674(93)80070-U)

Guy, C.S., K.M. Vignali, J. Temirov, M.L. Bettini, A.E. Overacre, M. Smeltzer, H. Zhang, J.B. Huppa, Y.H. Tsai, C. Lobry, et al. 2013. Distinct TCR signaling pathways drive proliferation and cytokine production in T cells. *Nat. Immunol.* 14:262–270. <https://doi.org/10.1038/ni.2538>

Irving, B.A., F.W. Alt, and N. Killeen. 1998. Thymocyte development in the absence of pre-T cell receptor extracellular immunoglobulin domains. *Science.* 280:905–908. <https://doi.org/10.1126/science.280.5365.905>

Janas, M.L., G. Varano, K. Gudmundsson, M. Noda, T. Nagasawa, and M. Turner. 2010. Thymic development beyond beta-selection requires phosphatidylinositol 3-kinase activation by CXCR4. *J. Exp. Med.* 207: 247–261. <https://doi.org/10.1084/jem.20091430>

Kageyama, R., T. Ohtsuka, and T. Kobayashi. 2007. The Hes gene family: repressors and oscillators that orchestrate embryogenesis. *Development.* 134:1243–1251. <https://doi.org/10.1242/dev.000786>

Klein, F., M. Mitrovic, J. Roux, C. Engdahl, L. von Muenchow, L. Alberti-Servera, H.J. Fehling, P. Pelczar, A. Rolink, and P. Tsapogas. 2019. The transcription factor Duxbl mediates elimination of pre-T cells that fail  $\beta$ -selection. *J. Exp. Med.* 216:638–655. <https://doi.org/10.1084/jem.20181444>

Koller, B.H., P. Marrack, J.W. Kappler, and O. Smithies. 2010. Normal development of mice deficient in beta 2M, MHC class I proteins, and CD8+ T cells. 1990. *J. Immunol.* 184:4592–4595.

Kreslavsky, T., M. Gleimer, M. Miyazaki, Y. Choi, E. Gagnon, C. Murre, P. Sicinski, and H. von Boehmer. 2012.  $\beta$ -Selection-induced proliferation is required for  $\alpha\beta$  T cell differentiation. *Immunity.* 37:840–853. <https://doi.org/10.1016/j.immuni.2012.08.020>

Le Borgne, M., E. Ladi, I. Dzhagalov, P. Herzmark, Y.F. Liao, A.K. Chakraborty, and E.A. Robey. 2009. The impact of negative selection on

- thymocyte migration in the medulla. *Nat. Immunol.* 10:823–830. <https://doi.org/10.1038/ni.1761>
- Lee, K.H., A.D. Holdorf, M.L. Dustin, A.C. Chan, P.M. Allen, and A.S. Shaw. 2002. T cell receptor signaling precedes immunological synapse formation. *Science*. 295:1539–1542. <https://doi.org/10.1126/science.1067710>
- Lee, K.H., A.R. Dinner, C. Tu, G. Campi, S. Raychaudhuri, R. Varma, T.N. Sims, W.R. Burack, H. Wu, J. Wang, et al. 2003. The immunological synapse balances T cell receptor signaling and degradation. *Science*. 302:1218–1222. <https://doi.org/10.1126/science.1086507>
- Lee, J.B., T.E. Werbowetski-Ogilvie, J.-H. Lee, B.A.S. McIntyre, A. Schnerch, S.-H. Hong, I.-H. Park, G.Q. Daley, I.D. Bernstein, and M. Bhatia. 2013. Notch-HES1 signaling axis controls hemato-endothelial fate decisions of human embryonic and induced pluripotent stem cells. *Blood*. 122:1162–1173. <https://doi.org/10.1182/blood-2012-12-471649>
- Levelt, C.N., P. Mombaerts, B. Wang, H. Kohler, S. Tonegawa, K. Eichmann, and C. Terhorst. 1995. Regulation of thymocyte development through CD3: functional dissociation between p56lck and CD3 sigma in early thymic selection. *Immunity*. 3:215–222. [https://doi.org/10.1016/1074-7613\(95\)90091-8](https://doi.org/10.1016/1074-7613(95)90091-8)
- Love, P.E., and A. Bhandoola. 2011. Signal integration and crosstalk during thymocyte migration and emigration. *Nat. Rev. Immunol.* 11:469–477. <https://doi.org/10.1038/nri2989>
- Ludford-Menting, M.J., J. Oliaro, F. Sacirbegovic, E.T. Cheah, N. Pedersen, S.J. Thomas, A. Pasam, R. Iazzolino, L.E. Dow, N.J. Waterhouse, et al. 2005. A network of PDZ-containing proteins regulates T cell polarity and morphology during migration and immunological synapse formation. *Immunity*. 22:737–748. <https://doi.org/10.1016/j.immuni.2005.04.009>
- Lukinavičius, G., L. Reymond, E. D'Este, A. Masharina, F. Göttfert, H. Ta, A. Güther, M. Fournier, S. Rizzo, H. Waldmann, et al. 2014. Fluorogenic probes for live-cell imaging of the cytoskeleton. *Nat. Methods*. 11:731–733. <https://doi.org/10.1038/nmeth.2972>
- Mahtani-Patching, J., J.F. Neves, D.J. Pang, K.V. Stoenchev, A.M. Aguirre-Blanco, B. Silva-Santos, and D.J. Pennington. 2011. PreTCR and TCR $\gamma\delta$  signal initiation in thymocyte progenitors does not require domains implicated in receptor oligomerization. *Sci. Signal*. 4:ra47. <https://doi.org/10.1126/scisignal.2001765>
- Maillard, I., L. Tu, A. Sambandam, Y. Yashiro-Ohtani, J. Millholland, K. Keeshan, O. Shestova, L. Xu, A. Bhandoola, and W.S. Pear. 2006. The requirement for Notch signaling at the beta-selection checkpoint in vivo is absolute and independent of the pre-T cell receptor. *J. Exp. Med.* 203:2239–2245. <https://doi.org/10.1084/jem.20061020>
- Mallick, C.A., E.C. Dudley, J.L. Viney, M.J. Owen, and A.C. Hayday. 1993. Rearrangement and diversity of T cell receptor beta chain genes in thymocytes: a critical role for the beta chain in development. *Cell*. 73:513–519. [https://doi.org/10.1016/0092-8674\(93\)90138-G](https://doi.org/10.1016/0092-8674(93)90138-G)
- Mallis, R.J., K. Bai, H. Arthanari, R.E. Hussey, M. Handley, Z. Li, L. Chingozha, J.S. Duke-Cohan, H. Lu, J.H. Wang, et al. 2015. Pre-TCR ligand binding impacts thymocyte development before  $\alpha\beta$ TCR expression. *Proc. Natl. Acad. Sci. USA*. 112:8373–8378. <https://doi.org/10.1073/pnas.1504971112>
- Martín-Cófreces, N.B., J. Robles-Valero, J.R. Cabrero, M. Mittelbrunn, M. Gordón-Alonzo, C.-H. Sung, B. Alarcón, J. Vázquez, and F. Sánchez-Madrid. 2008. MTOC translocation modulates IS formation and controls sustained T cell signaling. *J. Cell Biol.* 182:951–962. <https://doi.org/10.1083/jcb.200801014>
- Martín-Cófreces, N.B., B. Alarcón, and F. Sánchez-Madrid. 2011. Tubulin and actin interplay at the T cell and antigen-presenting cell interface. *Front. Immunol.* 2:24. <https://doi.org/10.3389/fimmu.2011.00024>
- Michie, A.M., and J.C. Zúñiga-Pflücker. 2002. Regulation of thymocyte differentiation: pre-TCR signals and beta-selection. *Semin. Immunol.* 14:311–323. [https://doi.org/10.1016/S1044-5323\(02\)00064-7](https://doi.org/10.1016/S1044-5323(02)00064-7)
- Mittelbrunn, M., C. Gutiérrez-Vázquez, C. Villarroya-Beltri, S. González, F. Sánchez-Cabo, M.Á. González, A. Bernad, and F. Sánchez-Madrid. 2011. Unidirectional transfer of microRNA-loaded exosomes from T cells to antigen-presenting cells. *Nat. Commun.* 2:282. <https://doi.org/10.1038/ncomms1285>
- Miyazaki, M., K. Miyazaki, M. Itoi, Y. Katoh, Y. Guo, R. Kanno, Y. Katoh-Fukui, H. Honda, T. Amagai, M. van Lohuizen, et al. 2008. Thymocyte proliferation induced by pre-T cell receptor signaling is maintained through polycomb gene product Bmi-1-mediated Cdkn2a repression. *Immunity*. 28:231–245. <https://doi.org/10.1016/j.immuni.2007.12.013>
- Pang, S.S., R. Berry, Z. Chen, L. Kjer-Nielsen, M.A. Perugini, G.F. King, C. Wang, S.H. Chew, N.L. La Gruta, N.K. Williams, et al. 2010. The structural basis for autonomous dimerization of the pre-T-cell antigen receptor. *Nature*. 467:844–848. <https://doi.org/10.1038/nature09448>
- Pardoll, D.M., B.J. Fowlkes, J.A. Bluestone, A. Kruisbeek, W.L. Maloy, J.E. Coligan, and R.H. Schwartz. 1987. Differential expression of two distinct T-cell receptors during thymocyte development. *Nature*. 326:79–81. <https://doi.org/10.1038/326079a0>
- Petrie, H.T., M. Tourigny, D.B. Burtrum, and F. Livak. 2000. Precursor thymocyte proliferation and differentiation are controlled by signals unrelated to the pre-TCR. *J. Immunol.* 165:3094–3098. <https://doi.org/10.4049/jimmunol.165.6.3094>
- Pham, K., R. Shimoni, M.J. Ludford-Menting, C.J. Nowell, P. Lobachevsky, Z. Bomzon, M. Gu, T.P. Speed, C.J. McClade, and S.M. Russell. 2013. Divergent lymphocyte signalling revealed by a powerful new tool for analysis of time-lapse microscopy. *Immunol. Cell Biol.* 91:70–81. <https://doi.org/10.1038/icb.2012.49>
- Pham, K., R. Shimoni, M. Charnley, M.J. Ludford-Menting, E.D. Hawkins, K. Ramsbottom, J. Oliaro, D. Izon, S.B. Ting, J. Reynolds, et al. 2015. Asymmetric cell division during T cell development controls downstream fate. *J. Cell Biol.* 210:933–950. <https://doi.org/10.1083/jcb.201502053>
- Raulet, D.H., R.D. Garman, H. Saito, and S. Tonegawa. 1985. Developmental regulation of T-cell receptor gene expression. *Nature*. 314:103–107. <https://doi.org/10.1038/314103a0>
- Rothenberg, E.V., J.E. Moore, and M.A. Yui. 2008. Launching the T-cell-lineage developmental programme. *Nat. Rev. Immunol.* 8:9–21. <https://doi.org/10.1038/nri2232>
- Ryser, J.E., E. Rungger-Brändle, C. Chaponnier, G. Gabbiani, and P. Vassalli. 1982. The area of attachment of cytotoxic T lymphocytes to their target cells shows high motility and polarization of actin, but not myosin. *J. Immunol.* 128:1159–1162.
- Saint-Ruf, C., M. Panigada, O. Azogui, P. Debey, H. von Boehmer, and F. Grassi. 2000. Different initiation of pre-TCR and gammadeltaTCR signalling. *Nature*. 406:524–527. <https://doi.org/10.1038/35020093>
- Schmitt, T.M., and J.C. Zúñiga-Pflücker. 2002. Induction of T cell development from hematopoietic progenitor cells by delta-like-1 in vitro. *Immunity*. 17:749–756. [https://doi.org/10.1016/S1074-7613\(02\)00474-0](https://doi.org/10.1016/S1074-7613(02)00474-0)
- Shinkai, Y., A. Ma, H.L. Cheng, and F.W. Alt. 1995. CD3 epsilon and CD3 zeta cytoplasmic domains can independently generate signals for T cell development and function. *Immunity*. 2:401–411. [https://doi.org/10.1016/1074-7613\(95\)90148-5](https://doi.org/10.1016/1074-7613(95)90148-5)
- Smith-Garvin, J.E., G.A. Koretzky, and M.S. Jordan. 2009. T cell activation. *Annu. Rev. Immunol.* 27:591–619. <https://doi.org/10.1146/annurev.immunol.021908.132706>
- Tahara, E., H. Kadara, L. Lacroix, D. Lotan, and R. Lotan. 2009. Activation of protein kinase C by phorbol 12-myristate 13-acetate suppresses the growth of lung cancer cells through KLF6 induction. *Cancer Biol. Ther.* 8:801–807. <https://doi.org/10.4161/cbt.8.9.8186>
- Tramont, P.C., A.-C. Tosello-Tramont, Y. Shen, A.K. Duley, A.E. Sutherland, T.P. Bender, D.R. Littman, and K.S. Ravichandran. 2010. CXCR4 acts as a costimulator during thymic  $\beta$ -selection. *Nat. Immunol.* 11:162–170. <https://doi.org/10.1038/ni.1830>
- Tsun, A., I. Qureshi, J.C. Stinchcombe, M.R. Jenkins, M. de la Roche, J. Kleczkowska, R. Zamoyka, and G.M. Griffiths. 2011. Centrosome docking at the immunological synapse is controlled by Lck signaling. *J. Cell Biol.* 192:663–674. <https://doi.org/10.1083/jcb.201008140>
- Turner, S.J., P.C. Doherty, J. McCluskey, and J. Rossjohn. 2006. Structural determinants of T-cell receptor bias in immunity. *Nat. Rev. Immunol.* 6:883–894. <https://doi.org/10.1038/nri1977>
- von Boehmer, H. 2005. Unique features of the pre-T-cell receptor alpha-chain: not just a surrogate. *Nat. Rev. Immunol.* 5:571–577. <https://doi.org/10.1038/nri1636>
- Wolfer, A., A. Wilson, M. Nemir, H.R. MacDonald, and F. Radtke. 2002. Inactivation of Notch1 impairs VDJbeta rearrangement and allows pre-TCR-independent survival of early  $\alpha\beta$  Lineage Thymocytes. *Immunity*. 16:869–879. [https://doi.org/10.1016/S1074-7613\(02\)00330-8](https://doi.org/10.1016/S1074-7613(02)00330-8)
- Yamasaki, S., and T. Saito. 2007. Molecular basis for pre-TCR-mediated autonomous signaling. *Trends Immunol.* 28:39–43. <https://doi.org/10.1016/j.it.2006.11.006>
- Yamasaki, S., E. Ishikawa, M. Sakuma, K. Ogata, K. Sakata-Sogawa, M. Hiroshima, D.L. Wiest, M. Tokunaga, and T. Saito. 2006. Mechanistic basis of pre-T cell receptor-mediated autonomous signaling critical for thymocyte development. *Nat. Immunol.* 7:67–75. <https://doi.org/10.1038/ni1290>
- Yashiro-Ohtani, Y., Y. He, T. Ohtani, M.E. Jones, O. Shestova, L. Xu, T.C. Fang, M.Y. Chiang, A.M. Intlekofer, S.C. Blacklow, et al. 2009. Pre-TCR signaling inactivates Notch1 transcription by antagonizing E2A. *Genes Dev.* 23:1665–1676. <https://doi.org/10.1101/gad.1793709>
- Zhao, B., K. Yoganathan, L. Li, J.Y. Lee, J.C. Zúñiga-Pflücker, and P.E. Love. 2019. Notch and the pre-TCR coordinate thymocyte proliferation by induction of the SCF subunits Fbx11 and Fbx12. *Nat. Immunol.* 20:1381–1392.

Supplemental material

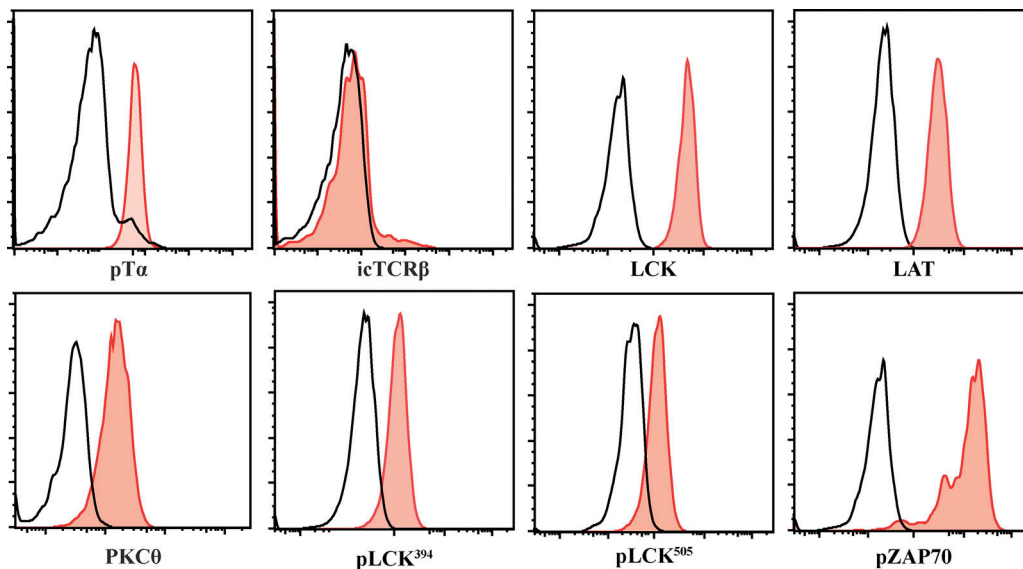


Figure S1. **Early DN3 cells (DN3a) express pre-TCR structural and signaling molecules.** Primary T cell precursors from mouse fetal liver were cocultured for 9 d with OP9-DL1 stromal cells. DN3a cells were purified from the coculture and assessed for the levels of expression and phosphorylation of the pre-TCR structural and signaling molecules, as shown by the histograms. The black line indicates Alexa Fluor 647 staining without primary antibody, and the red lines are the pre-TCR-associated proteins. The results are representative of three independent experiments.

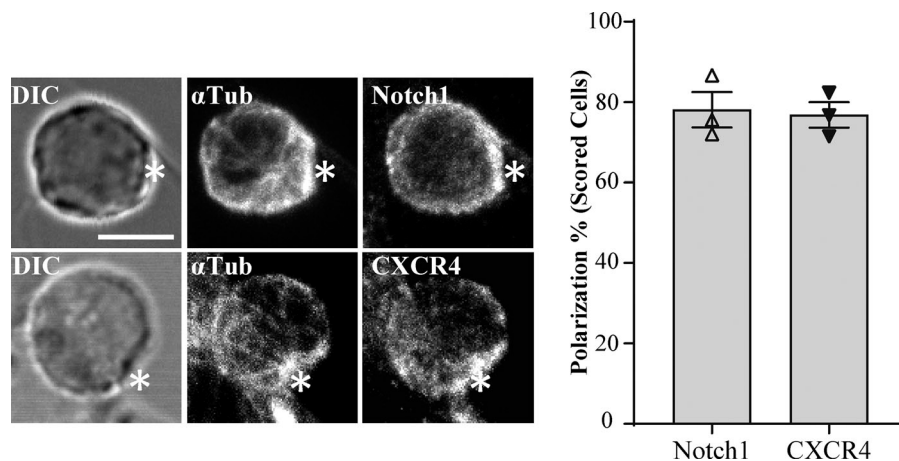


Figure S2. **Notch1 and CXCR4 polarize at the interface between DN3a and OP9-DL1 stromal cells.** DN3 cells were incubated with OP9-DL1 cells for 14 h and then fixed and stained for  $\alpha$ -tubulin to mark the MTOC and either Notch1 or CXCR4 (as shown). Maximum projection of z-stack images were acquired using confocal microscopy, and representative images are shown. After triaging for cells in which the MTOC was recruited to the interface (indicated by asterisks) with an OP9-DL1 cell, the percentage of cells in which Notch1 and CXCR4 were polarized to the interface with the OP9-DL1 cell was determined by blind scoring (as shown by column-bar plot). The total number of scored conjugates per marker is 75 (25 cells per biological replicate). Scale bar, 5  $\mu$ m. Error bars represent SEM.

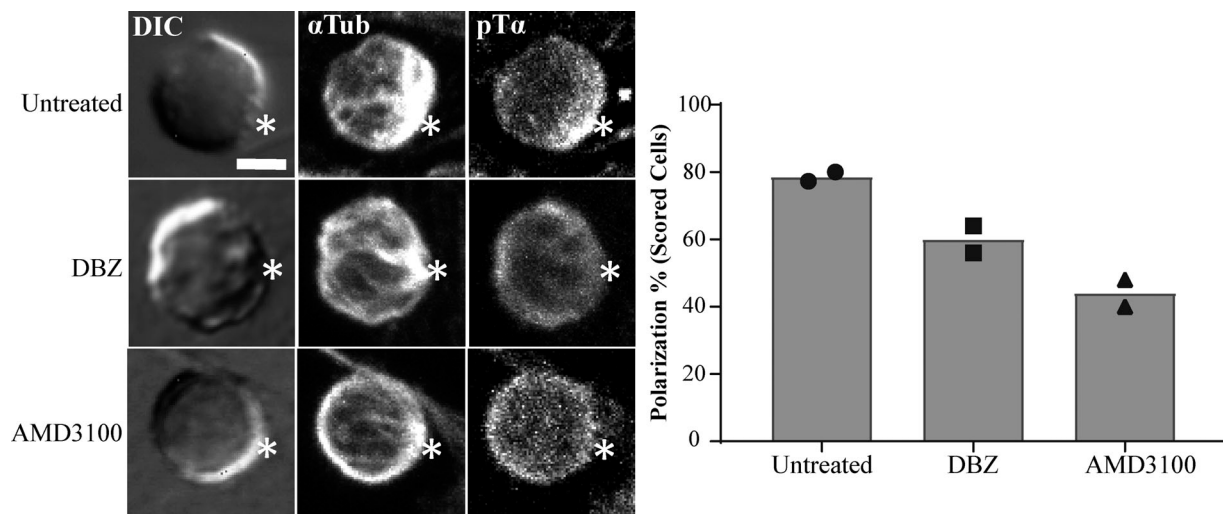
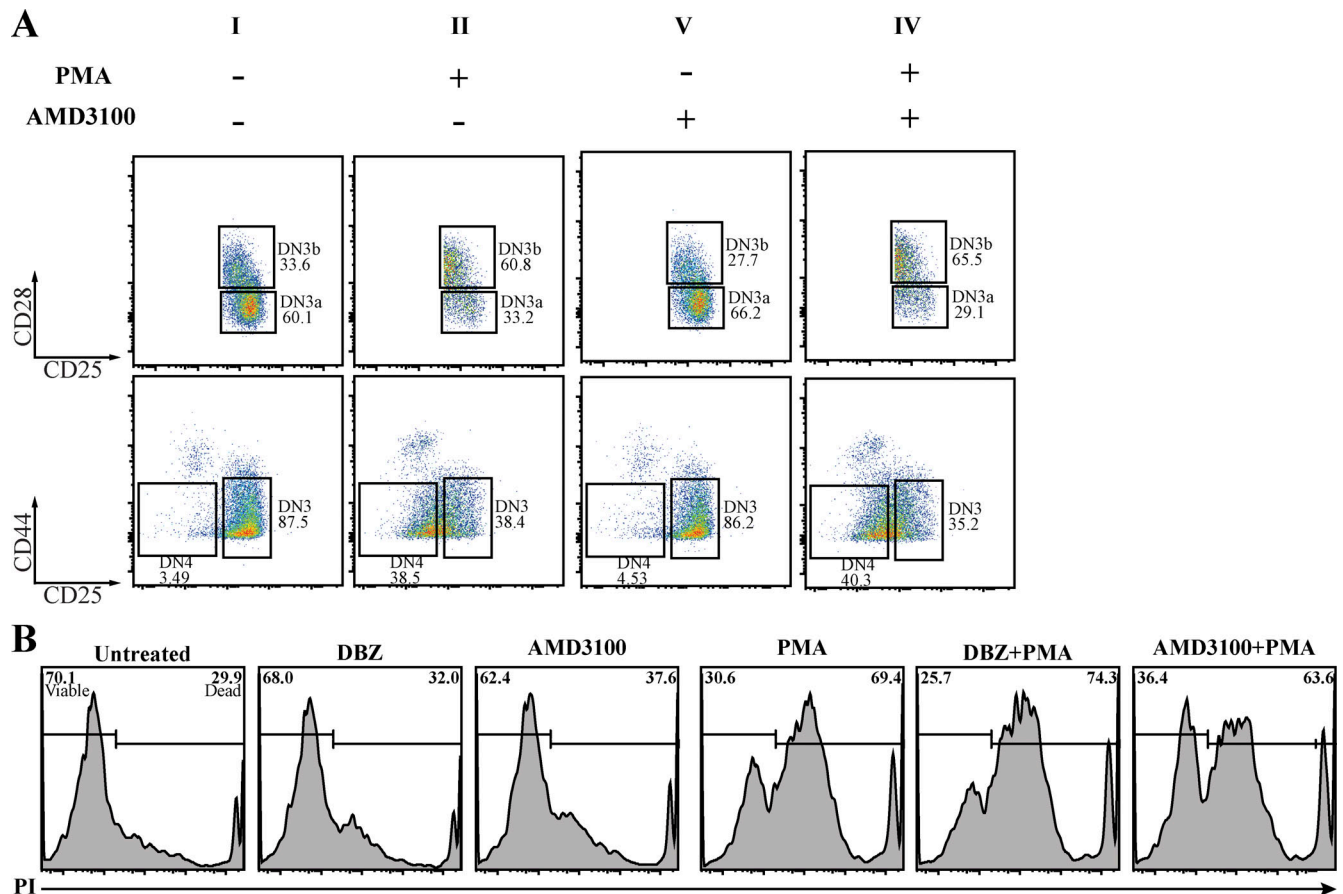


Figure S3. **Inhibition of Notch and CXCR4 for 3 h disrupts immunological synapse formation in vitro.** Purified DN3a cells were incubated with OP9-DL1 cells for 3 h in the presence or absence of either Notch inhibitor (DBZ) or CXCR4 inhibitor (AMD3100) and then fixed and stained for  $\alpha$ -tubulin to mark the MTOC and pT $\alpha$  chain as a marker of pre-TCR (as shown). After triaging for cells in which the MTOC was recruited to the interface (white asterisks) with an OP9-DL1 cell, the percentage of cells in which pT $\alpha$  was polarized to the interface with the OP9-DL1 cell was determined by blind scoring (as shown by column-bar plot). The total number of scored conjugates per condition is 50 (25 cells per biological replicate). Scale bar, 5  $\mu$ m.



**Figure S4. The effect of inhibition of CXCR4 signaling on progression beyond  $\beta$ -selection indicates a role in immunological synapse assembly. (A)** Purified TCR $\beta^-$  DN3a cells were cocultured on OP9-DL1 cells in the presence or absence of either of the following drug combinations: Notch inhibitor (DBZ), CXCR4 inhibitor (AMD3100), a pharmacological mimic of pre-TCR downstream signaling molecule (PMA), PMA with Notch inhibitor, and PMA with CXCR4 inhibitor. Cocultures were stopped after 48 h, and PI was used to assess the effect of each treatment on survival (as shown by histograms). **(B)** Purified TCR $\beta^-$  DN3a cells were cocultured on OP9-DL1 cells in the presence or absence of either of the following drug combinations: CXCR4 inhibitor (AMD3100), a pharmacological mimic of pre-TCR downstream signaling (PMA), and PMA with CXCR4 inhibitor. Cocultures were stopped after 48 h and analyzed by flow cytometry to assess progression and differentiation (as shown by flow cytometry dot plots). The presented data are representative of three independent biological replicates with similar results.

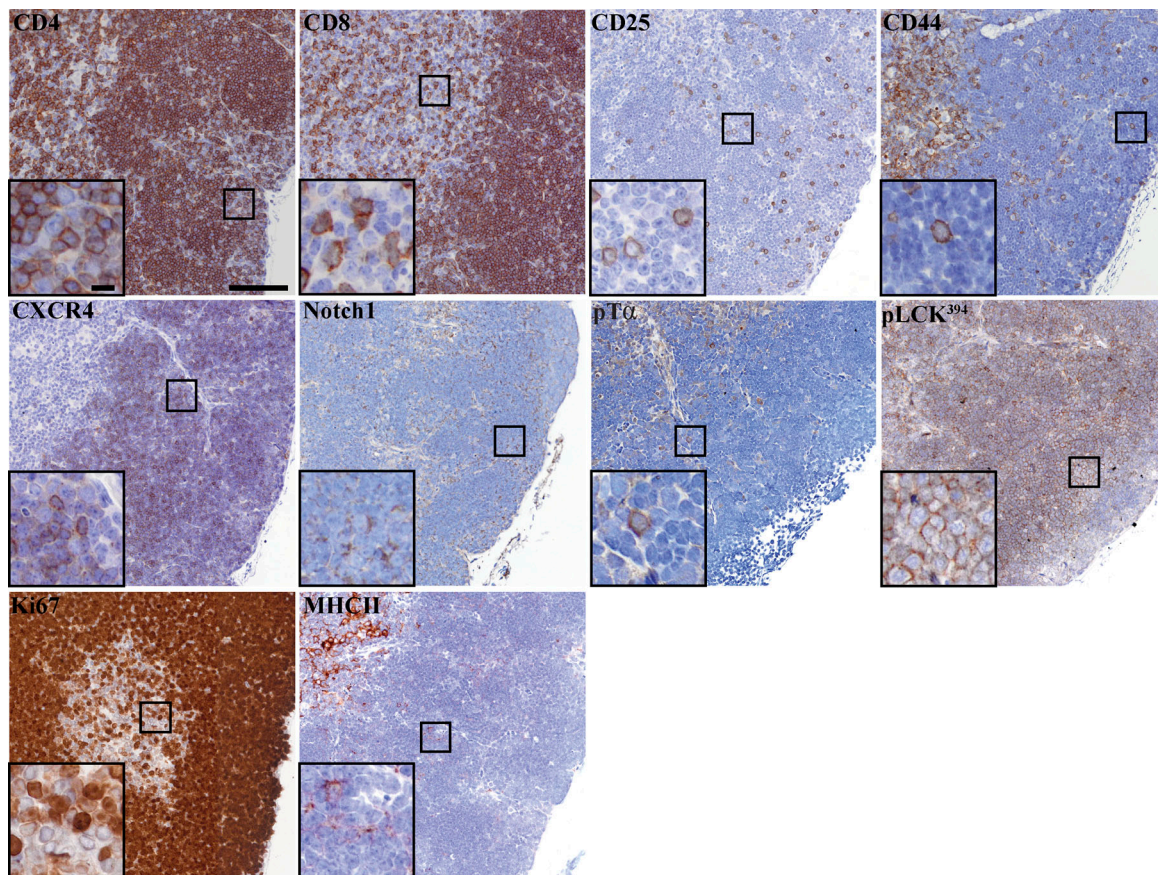


Figure S5. **Chromogenic detection of markers used in Opal multiplex.** Thymus lobe slices of 4  $\mu\text{m}$  thickness were mounted on a glass slide, and chromogenic detection (brown) of the multiplex thymus panel markers was performed, followed by counterstaining with hematoxylin to visualize the nucleus (blue). Images were acquired using an Olympus V120 slide scanner, and representative images are shown. Scale bar, 100  $\mu\text{m}$  (10  $\mu\text{m}$  in zoomed images).

Video 1. **F-actin relocates to the front of DN3a cells upon docking onto OP-DL1.** Time-lapse confocal microscopy showing DN3a cell stained with SiR-Actin (red, top right frame) cocultured with OP-DL1 cells (green, top left). Top left: SiR-Actin polarizes and stabilizes at the interface between DN3 and OP-DL1 cells (green, top right frame) for a period of  $\sim 54$  min ( $n = 22$ ). Bottom left: DIC of field of view; bottom right: merge of the SiR-Actin and DIC frames. Each frame is 3 min, and playback is 3 frames per second.

Video 2. **DN3a cells form an immunological synapse upon docking onto OP-DL1 cells.** Time-lapse confocal microscopy showing polarization of the pre-TCR components, including  $\alpha$ -tubulin (cyan, top right), LAT (purple, top middle), and SiR-Actin (white, bottom middle) at the interface between DN3a and OP-DL1 cells ( $n = 14$ ). The top right frame shows a merge of  $\alpha$ -tubulin (cyan) and LAT (purple) frames, the bottom left shows a DIC frame of the field of view, and the bottom right shows a merge of LAT (cyan) and SiR-Actin (white). Each frame is 3 min, and playback is 3 frames per second.

Provided online are two tables. Table S1 lists antibodies used in flow cytometry and immunofluorescence. Table S2 lists antibodies used in the thymus multiplex antibodies panel.